ATLAS CONF Note

ATLAS-CONF-2023-029

22nd May 2023

Search for electroweak SUSY production in final states with two τ-leptons in $\sqrt{s} = 13$ TeV pp collisions with the ATLAS detector

The ATLAS Collaboration

Three searches for the direct production of staus or charginos and neutralinos in final states with at least two hadronically decaying τ-leptons are presented. For chargino and neutralino production, decays via intermediate staus or Wh bosons are considered. The analysis uses a dataset of pp collisions corresponding to an integrated luminosity of 139 fb^{-1}, recorded with the ATLAS detector at the Large Hadron Collider at a centre-of-mass energy of 13 TeV. No significant deviation from the expected Standard Model background is observed and SUSY particle mass limits at 95 % confidence level are obtained in simplified models. For direct production of $\tilde{\chi}_1^+\tilde{\chi}_1^-$, chargino masses are excluded up to 970 GeV, while $\tilde{\chi}_1^\pm$ and $\tilde{\chi}_2^0$ masses up to 1160 GeV (330 GeV) are excluded for $\tilde{\chi}_1^\pm\tilde{\chi}_2^0/\tilde{\chi}_1^+\tilde{\chi}_1^-$ production decaying via staus (Wh bosons). Stau masses up to 480 GeV are excluded for mass degenerate $\tilde{\tau}_{L,R}$ scenarios and up to 410 GeV for $\tilde{\tau}_L$-only scenarios. The first sensitivity to $\tilde{\tau}_R$-only scenarios is presented here, with $\tilde{\tau}_R$ masses excluded up to 330 GeV.

ATLAS-CONF-2023-029
06 June 2023

1 Introduction

Supersymmetry (SUSY) [1–7] postulates the existence of a bosonic (fermionic) partner for each fermionic (bosonic) particle of the Standard Model (SM), whose spin differs by one half unit from each corresponding SM particle. In models that conserve R-parity [8], the lightest supersymmetric particle (LSP) is stable and can be an excellent dark-matter candidate [9, 10].

In the simplified SUSY models considered here, the sector of SUSY particles with only electroweak interactions contains charginos ($\tilde{\chi}_i^{\pm}$, $i = 1, 2$, in order of increasing masses), neutralinos ($\tilde{\chi}_j^0$, $j = 1, 2, 3, 4$, in order of increasing masses), charged sleptons ($\tilde{\ell}$), and sneutrinos ($\tilde{\nu}$). Charginos and neutralinos are the mass eigenstates formed from linear superpositions of the superpartners of the Higgs bosons and electroweak gauge bosons. The charged sleptons are the superpartners of the charged leptons and in a similar convention as for the SM partners, referred to as $\tilde{\ell}_{\mathrm{L}}$ or $\tilde{\ell}_{\mathrm{R}}$, respectively. The slepton mass eigenstates are a mixture of $\tilde{\ell}_{\mathrm{L}}$ and $\tilde{\ell}_{\mathrm{R}}$, and are labeled as $\tilde{\ell}_k$ ($k = 1, 2$ in order of increasing mass). In this work, the scalar superpartners of the left-handed τ ($\tilde{\tau}_{\mathrm{L}}$) and right-handed τ ($\tilde{\tau}_{\mathrm{R}}$) are assumed to be mass degenerate unless explicitly stated, and are referred to as "staus".

Although they are experimentally challenging, final states with taus, τ, are of particular interest in SUSY searches. Light sleptons could play a role in the co-annihilation of neutralinos in the early universe, and models with light stau decays to light neutralinos can shed light on the nature of dark matter [11]. Furthermore, should SUSY or any other physics beyond the Standard Model (BSM) involving leptons be discovered, independent studies of all three lepton flavours are necessary to investigate the coupling structure of the new physics, especially with regard to lepton universality.

All SUSY scenarios considered in this publication conserve R-parity. The first SUSY scenario considered is the direct production of stau pairs, either with mass degenerate or non-degenerate $\tilde{\tau}_{\mathrm{L,R}}$, which decay directly to a tau and the LSP 100% of the time. The second scenario includes the production of neutralinos and charginos, $\tilde{\chi}_1^{\pm}\tilde{\chi}_2^0$ and $\tilde{\chi}_1^{+}\tilde{\chi}_1^{-}$, which decay to the lightest neutralino only through intermediate staus or tau sneutrinos with equal branching fraction, denoted as the "Intermediate stau" channel. The stau and sneutrino masses are assumed to be halfway between the $\tilde{\chi}_2^0/\tilde{\chi}_1^{\pm}$ and $\tilde{\chi}_1^0$ masses. The search for $\tilde{\chi}_1^{\pm}\tilde{\chi}_2^0$ production is separated into final states with two same-sign (SS) or opposite-sign (OS) τ pairs. The third SUSY scenario is the direct production of neutralinos and charginos, $\tilde{\chi}_1^{\pm}\tilde{\chi}_2^0$ which decay via the lightest neutral Higgs boson (h), consistent with the SM Higgs boson with a mass of 125 GeV, a W boson and two neutralinos. This scenario is referred to as the "Intermediate Wh" channel. For the third SUSY scenario, the final state is chosen to contain two hadronic taus from the Higgs boson decay and one charged light lepton (e, μ) from the W boson decay. The light lepton may be the result of a $W \rightarrow \tau\nu$ decay where the τ decays leptonically. For all three searches presented in this publication, the final state includes two hadronically decaying taus, low jet activity and large missing transverse momentum, $\mathbf{p}_{\mathrm{T}}^{\mathrm{miss}}$, from the neutralinos and neutrinos. Representative diagrams of the targeted signal processes can be found in Figure 1.

Previous results from the ATLAS experiment have set exclusion limits at 95% confidence level on the above SUSY models with the Run 1 and partial Run 2 datasets [12–15]. The CMS experiment also sets similar exclusion limits [16, 17]. This search aims to extend the current ATLAS reach to higher chargino masses and smaller mass differences between $\tilde{\chi}_2^0/\tilde{\chi}_1^{\pm}/\tilde{\tau}$ and $\tilde{\chi}_1^0$ using the increased statistics of the full Run 2 dataset, and achieve the first sensitivity to $\tilde{\tau}_R$ pair production scenarios by introducing the use of machine learning algorithms.

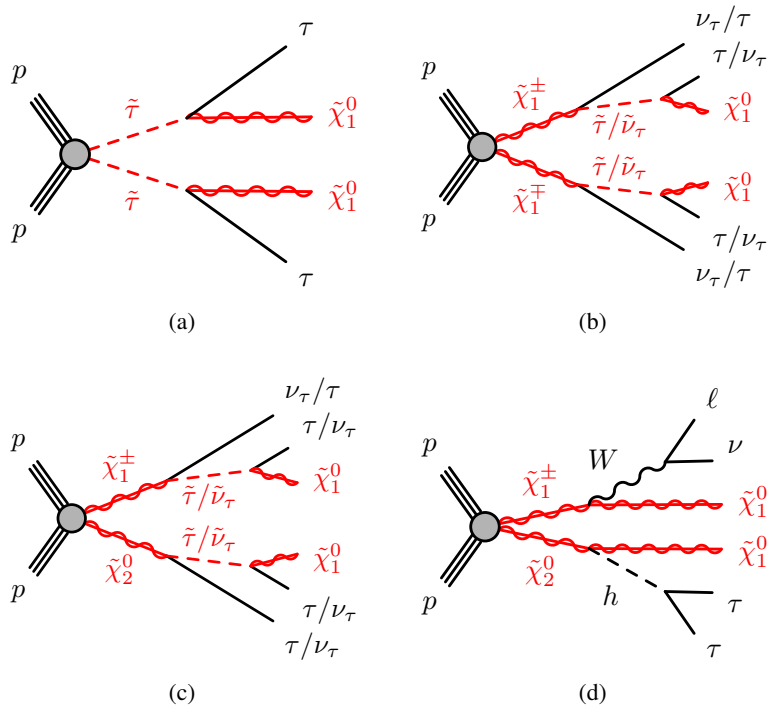

Figure 1: Representative diagrams of SUSY scenarios which are being searched for in this publication. Direct stau production is shown in (a), while (b) and (c) show the processes considered for the Intermediate stau channel. The process for the Intermediate Wh channel is shown in (d). In all cases, the subsequent decays contain a two τ final state. In the case of $\tilde{\chi}_1^{\pm}\tilde{\chi}_2^0$ production (c), the final state can contain more than two taus.

The publication is structured as follows: the ATLAS detector is briefly introduced in Section 2 followed by a description of the data and simulated samples used in Section 3 and the reconstruction of events in Section 4; the general analysis strategy is outlined in Section 5, followed by the details of the direct stau, intermediate stau, and intermediate Wh searches in Sections 6, 7, and 8, respectively; the systematic uncertainties are discussed in Section 9 and the results are presented in Section 10, before conclusions are drawn in Section 11.

2 ATLAS detector

The ATLAS experiment [18] at the LHC is a multipurpose particle detector with a forward–backward symmetric cylindrical geometry and a near 4π coverage in solid angle.[1] It consists of an inner tracking detector (ID) surrounded by a thin superconducting solenoid providing a 2 T axial magnetic field, electromagnetic and hadron calorimeters, and a muon spectrometer. The inner tracking detector covers the pseudorapidity range $|\eta| < 2.5$. It consists of silicon pixel, silicon microstrip, and transition radiation

[1] ATLAS uses a right-handed coordinate system with its origin at the nominal interaction point (IP) in the centre of the detector and the z-axis along the beam pipe. The x-axis points from the IP to the centre of the LHC ring, and the y-axis points upwards. Cylindrical coordinates (r, ϕ) are used in the transverse plane, ϕ being the azimuthal angle around the z-axis. The pseudorapidity is defined in terms of the polar angle θ as $\eta = -\ln\tan(\theta/2)$. Angular distance is measured in units of $\Delta R \equiv \sqrt{(\Delta\eta)^2 + (\Delta\phi)^2}$.

tracking detectors. Lead/liquid-argon (LAr) sampling calorimeters provide electromagnetic (EM) energy measurements with high granularity. A steel/scintillator-tile hadron calorimeter covers the central pseudorapidity range ($|\eta| < 1.7$). The endcap and forward regions are instrumented with LAr calorimeters for both the EM and hadronic energy measurements up to $|\eta| = 4.9$. The muon spectrometer (MS) surrounds the calorimeters and is based on three large superconducting air-core toroidal magnets with eight coils each. The field integral of the toroids ranges between 2.0 and 6.0 T m across most of the detector. The muon spectrometer includes a system of precision tracking chambers and fast detectors for triggering. A two-level trigger system is used to select events. The first-level trigger is implemented in hardware and uses a subset of the detector information to accept events at a rate below 100 kHz. This is followed by a software-based trigger that reduces the accepted event rate to 1 kHz on average depending on the data-taking conditions. An extensive software suite [19] is used in the reconstruction and analysis of real and simulated data, in detector operations, and in the trigger and data acquisition systems of the experiment.

3 Data and simulated event samples

The dataset considered in this publication corresponds to 139 fb^{-1} of pp LHC collision data collected between 2015 and 2018 by the ATLAS detector, at a centre-of-mass energy of 13 TeV and with a 25 ns proton bunch crossing interval. Data quality requirements are imposed to ensure that only events in which the entire ATLAS detector was functioning well are used [20].

Simulated events produced with several Monte Carlo (MC) event generators are used to predict yields for background contributions from SM processes and for possible SUSY signals. To account for pile-up, all simulated events are overlaid with multiple pp collisions simulated with the soft QCD processes of Pythia 8.186 [21] using the A3 set of tuned parameters [22] and the NNPDF2.3lo leading order (LO) parton distribution functions (PDFs) [23]. For all samples showered with Pythia 8, EvtGen 1.2.0 [24] is used to simulate the decays of bottom and charmed hadrons. The simulated events are weighted such that the pile-up conditions match those of the data and are required to pass the trigger selections. The response of the detector to particles is modelled with an ATLAS detector simulation [25] based on Geant4 [26] for almost all SM background simulation; a few minor EWK Z+jet processes with very small yields for these searches use fast simulation based on a parameterisation of the performance of the ATLAS EM and hadronic calorimeters [27] and on Geant4 elsewhere.

Final states with two hadronically decaying taus, low jet activity and a large $\mathbf{p}_{\mathrm{T}}^{\mathrm{miss}}$ are included in this analysis. As a result, SM background processes containing both real and misidentified τ final state contributions are considered. These backgrounds are summarised in the following.

The production of top-quark pairs ($t\bar{t}$) and single top quarks in the Wt and s-channels is performed with Powheg Box v2 [28–31], with the NNPDF2.3lo [23] PDF set at next-to-leading order (NLO) in the Matrix elements (ME) calculations and the ATLAS underlying-event tune A14 [32]. Electroweak t-channel single-top-quark events are generated using the Powheg Box v2 event generator. The parton shower (PS), fragmentation, and the underlying event are simulated using Pythia 8.186 with the NNPDF2.3lo PDF set and a corresponding set of A14 tuned parameters. The top-quark mass is set to 172.5 GeV. The $t\bar{t}$ sample is normalised to the cross-section prediction at next-to-next-to-leading order (NNLO) in QCD including the resummation of next-to-next-to-leading logarithmic (NNLL) soft-gluon terms calculated using Top++ 2.0 [33–39]. The cross-section for single-top-quark is computed for the Wt-channel at NLO in QCD with NNLL soft gluon corrections [40, 41], and to NLO in QCD for the t- and s-channels [40, 41].

Top-quark pair production with an additional W or Z boson is calculated using aMC@NLO 2.2.2 [42] at NLO in the ME calculations, while fragmentation and hadronisation are simulated with Pythia 8.186. The underlying-event tune A14 is used with the NNPDF2.3lo PDF set, and the cross-sections are normalised using NLO predictions [43, 44].

Events with $Z/\gamma^* \to \ell\ell$ ($\ell = e, \mu, \tau$) and $W \to \ell\nu$ produced in association with jets (including jets initiated by heavy flavour quarks) are generated with Sherpa 2.2.1 [45, 46]. ME are calculated for up to two additional partons at NLO and four additional partons at LO, using the Comix [47] and OpenLoops [48, 49] generators and merged with the Sherpa PS [50] using the MENLOPS prescription [46]. The NNPDF3.0NNLO [51] PDF set is used in conjunction with a dedicated PS tuning developed by the Sherpa authors. The W/Z+jets events are normalised using their NNLO cross-sections [52].

Fully leptonically and semileptonically decaying diboson and tribsoson samples (VV and VVV, where $V = W, Z$) are simulated with the Sherpa 2.2.1 and Sherpa 2.2.2 [45] generator at NLO. In this setup, multiple matrix elements are matched and merged with the Sherpa parton shower based on Catani–Seymour dipole factorization [50] using the MENLOPS prescription [46, 53–55]. The virtual QCD corrections for matrix elements at NLO accuracy are provided by the OpenLoops library [49]. Samples are generated using the NNPDF3.0NNLO set, along with the dedicated set of tuned parton-shower parameters developed by the Sherpa authors.

Contributions from Higgs boson events produced by gluon–gluon fusion and vector-boson fusion are modelled using Powheg Box v2 with the NNPDF3.0NNLO PDF and showered using Pythia 8.186. Associated production of a Higgs boson with a vector boson and a Higgs boson in association with two top quarks are simulated using Pythia 8.186 and aMC@NLO, respectively. All Higgs boson samples are normalised to the cross-sections from Ref. [56].

SUSY signal model samples are generated to allow the interpretation of the search results in terms of SUSY parameters and are simulated using the ATLAS fast detector simulation. Signal samples are generated using aMC@NLO 2.2.3 interfaced to Pythia 8.186 with the A14 tune for the PS modelling, hadronisation, and underlying event. The ME calculation is performed at tree level and includes the emission of up to two additional partons. The PDF set used for the generation is NNPDF2.3lo. The ME–PS merging uses the CKKW-L [57] prescription, with a matching scale set to one quarter of the mass of the pair of produced particles. Signal cross-sections are calculated with Resummino v2.0.1 to NLO in the strong coupling constant, adding the resummation of soft gluon emission at next-to-leading-logarithm accuracy (NLO+NLL) [58, 59]. The nominal cross-section and the uncertainty are taken from an envelope of cross-section predictions using different PDF sets and factorisation and renormalisation scales, as described in Ref. [60].

4 Event reconstruction

After data quality requirements have been applied, events with at least one reconstructed primary vertex [61] are selected. A primary vertex is defined to have at least two associated charged-particle tracks with transverse momentum $p_{\mathrm{T}} > 500\,\mathrm{MeV}$ and be consistent with the beam spot envelope. If there are multiple primary vertices in an event, the one with the largest $\sum p_{\mathrm{T}}^2$ of the associated tracks is chosen.

Jets are reconstructed from particle-flow objects calibrated at the electromagnetic scale [62] using the anti-k_t algorithm [63, 64] with a radius parameter of 0.4. Jet energies are corrected for detector inhomogeneities, the non-compensating response of the calorimeter, and pile-up effects [65, 66]. The impact due to pile-up is

accounted for using a technique based on jet areas, that provides an event-by-event and jet-by-jet correction [67]. Jets that are likely to have originated from pile-up are not considered in the analysis[68]. Jets are required to have $p_{\mathrm{T}} > 20\,\mathrm{GeV}$ and $|\eta| < 2.8$ and events containing jets that are likely to have arisen from detector noise or cosmic rays are removed [69].

Jets containing b-hadrons (b-jets) are identified using the *DL1r* algorithm [70, 71], a multivariate discriminant making use of track impact parameters and reconstructed secondary vertices. Candidate b-jets are required to have $|\eta| < 2.5$. A working point is used that has a p_{T}-independent b-tagging efficiency of 77 % and light-jet (c-jet) rejection factor of 140 (4), based on studies using simulated $t\bar{t}$ events.

Electron candidates are reconstructed by matching clusters in the electromagnetic calorimeter with charged-particle tracks in the ID. Electrons are required to have $p_{\mathrm{T}} > 10\,\mathrm{GeV}$, $|\eta| < 2.47$, and to satisfy the "loose" working point according to a likelihood-based identification algorithm of Ref. [72]. Muon candidates are reconstructed from MS tracks matching ID tracks; they are required to have $p_{\mathrm{T}} > 10\,\mathrm{GeV}$ and $|\eta| < 2.7$ and fulfil the "medium" quality criteria of Ref. [73]. Events containing a muon candidate with a poorly measured charge-to-momentum ratio ($\sigma(q/p) \,/\, |q/p| > 0.2$) are rejected. Events are required not to contain any candidate muon with large transverse (d_0) and longitudinal (z_0) impact parameter, $|z_0| > 1\,\mathrm{mm}$ or $|d_0| > 0.2\,\mathrm{mm}$, in order to reduce contributions from those originating from cosmic rays. The efficiencies for electrons and muons to satisfy the reconstruction, identification, and isolation criteria are measured using samples of leptonic Z and J/ψ decays, and corrections are applied to the simulated samples to reproduce the efficiencies observed in data [72, 73].

The reconstruction of hadronically decaying taus is based on information from tracks in the ID and three-dimensional clusters in the electromagnetic and hadronic calorimeters. The tau reconstruction algorithm is seeded by jets reconstructed from topological clusters of energy deposits in the calorimeter and uses a looser requirement of $p_{\mathrm{T}} > 10\,\mathrm{GeV}$ and $|\eta| < 2.5$. The reconstructed energies of the hadronically decaying τ candidates are corrected from the local hadron topocluster scale to the tau energy scale, which is calibrated based on simulation and in-situ measurements using $Z \to \tau\tau$ decays [74]. Hadronic tau-decay candidates are required to have one or three associated charged-particle tracks (prongs) and the total electric charge of those tracks must be ± 1 times the electron charge. To improve the discrimination between hadronically decaying taus and jets, electrons, or muons, multivariate algorithms are used [75]. A recurrent neural network discriminant is used to reject jets that do not originate from a hadronically decaying τ with a "medium" or "tight" working point [76]. A boosted decision tree is used to discriminate 1-prong τ candidates against electrons. This discriminant is built using information from the EM calorimeter and the tracking detector. This requirement has about 95 % efficiency, and a rejection factor from 10 to 50 depending on the η range. τ candidates are required to have $p_{\mathrm{T}} > 20\,\mathrm{GeV}$ and $|\eta| < 2.47$, and must lie outside the transition region between the barrel and end-cap calorimeters ($1.37 < |\eta| < 1.52$).

The MC simulation is corrected for differences in the efficiencies of the tau identification at both trigger and reconstruction level between data and simulation. For hadronically decaying taus originating from prompt gauge boson decays, the corrections are calculated with a *tag-and-probe* method in a sample of $Z \to \tau\tau$ events where one τ decays hadronically and the other leptonically into a muon and two neutrinos [77].

The measured $\mathbf{p}_{\mathrm{T}}^{\mathrm{miss}}$, and its magnitude $E_{\mathrm{T}}^{\mathrm{miss}}$, is defined as the negative vectorial sum of the $\mathbf{p}_{\mathrm{T}}$ of all identified jets, τ candidates, electrons, photons, muons, and an additional soft term. The soft term is constructed from all tracks that are associated with the primary vertex but not with any identified particle or jet [78, 79].

To avoid the possible double counting of reconstructed objects, an overlap removal procedure is used, following these steps. The τ candidates that are close to electron or muon candidates ($\Delta R < 0.2$, where

$\Delta R = \sqrt{(\Delta y)^2 + (\Delta\phi)^2}$) are removed, as are electrons that share a track with a muon. For electrons close to a jet ($\Delta R < 0.4$), the electron is removed, except when $\Delta R < 0.2$ and the jet is not b-tagged, in which case the jet is removed. Any remaining jet within $\Delta R = 0.4$ of a muon or τ candidate is removed.

5 General analysis strategy and event variables

Events for all scenarios are required to have at least two hadronically decaying taus. Different Signal regions (SR) are defined to target the specific SUSY scenario, using kinematic variables that provide a good signal-to-background separation, described in this section. For taus, kinematic variables are calculated from the visible decay products. The event selections and background estimations are described for direct stau production SRs in Section 6, for the intermediate stau channel SRs in Section 7, and for the intermediate Wh channel SRs in Section 8.

The main SM backgrounds are estimated by normalising MC simulation samples to data in dedicated control regions (CRs); backgrounds resulting from non-prompt and misidentified leptons are derived from data, while sub-dominant backgrounds are estimated using MC simulation only. To validate the modelling of the SM backgrounds, the yields and shapes of key kinematic variables are compared to data in dedicated validation regions (VR). SRs are designed for the best expected sensitivity in the simplified SUSY signal models studied. Where appropriate, looser, or merged SRs are used to enhance discovery prospects or set model-independent limits.

The following variables are used to discriminate SUSY signals from the SM background:

- the "stransverse mass", m_{T2}, which has a kinematic endpoint for events where two massive pair produced particles each decay to a detected object (the lepton) and an undetected object (the neutralino) [80, 81]. It is defined as:

$$m_{\mathrm{T2}} = \min_{\mathbf{q}_{\mathrm{T}}} \left[\max \left(m_{\mathrm{T}}(\mathbf{p}_{\mathrm{T1}}, \mathbf{q}_{\mathrm{T}}), m_{\mathrm{T}}(\mathbf{p}_{\mathrm{T2}}, \mathbf{p}_{\mathrm{T}}^{\mathrm{miss}} - \mathbf{q}_{\mathrm{T}}) \right) \right],$$

  where $\mathbf{p}_{\mathrm{T1}}$ and $\mathbf{p}_{\mathrm{T2}}$ are the transverse momenta of the two leptons and $\mathbf{q}_{\mathrm{T}}$ is the transverse vector chosen to minimise the larger of the two transverse masses. They are defined by

$$m_{\mathrm{T}}(\mathbf{p}_{\mathrm{T}}, \mathbf{q}_{\mathrm{T}}) = \sqrt{2(p_{\mathrm{T}} q_{\mathrm{T}} - \mathbf{p}_{\mathrm{T}} \cdot \mathbf{q}_{\mathrm{T}})},$$

  where $\mathbf{q}_{\mathrm{T}}$ may be replaced by $\mathbf{p}_{\mathrm{T}}^{\mathrm{miss}} - \mathbf{q}_{\mathrm{T}}$ in the m_{T2} calculation, or by $\mathbf{p}_{\mathrm{T}}^{\mathrm{miss}}$ for the more straightforward transverse mass calculations. In events with more than two taus candidates, the pair that maximises $m_{\mathrm{T2}}$are used. Similarly, in the intermediate Wh analysis, the pairing of light lepton-τ or τ-τ the maximises m_{T2} is used. For $t\bar{t}$ and WW events, the m_{T2} distribution has a kinematic endpoint at the W boson mass, while for SUSY scenarios with large mass differences between the produced SUSY particle and the $\tilde{\chi}_1^0$, the m_{T2} distribution for signal events extends significantly beyond this endpoint. The $\tilde{\chi}_1^0$ is assumed to be massless in the calculation of m_{T2}.

- $m_{\mathrm{T},\ell}$, the transverse mass values obtained from the light lepton with the $\mathbf{p}_{\mathrm{T}}^{\mathrm{miss}}$, where ℓ can be e or μ.

- m_{Tsum}, the sum of the transverse mass values of the two highest-p_{T} τ candidates with the $\mathbf{p}_{\mathrm{T}}^{\mathrm{miss}}$. In the $\tilde{\chi}_1^{\pm}\tilde{\chi}_2^0$ with decays to an intermediate Wh scenario, m_{Tsum} also includes $m_{\mathrm{T}\ell}$.

- m_{eff}, the scalar sum of the $E_{\mathrm{T}}^{\mathrm{miss}}$ and the p_{T} of the two highest-p_{T} taus.

- $\Delta R(\tau_1, \tau_2) = \sqrt{(\Delta\eta(\tau_1, \tau_2)^2 + \Delta\phi(\tau_1, \tau_2)^2}$, the angular distance between the two highest-p_{T} taus. An upper requirement on this variable is used to discriminate against back-to-back objects in SM events.
- $m(\tau_1, \tau_2)$: the invariant mass of the two highest-p_{T} taus. A similar variable is also used for the invariant mass of a τ and a muon, $m(\tau, \mu)$.
- $|\Delta\phi(\tau_1, \tau_2)|$: the absolute value of the difference of azimuthal angle around the z-axis between the two highest-p_{T} τ candidates. A similar variable is also used for the $E_{\mathrm{T}}^{\mathrm{miss}}$ and taus, e.g. $|\Delta\phi(\tau, E_{\mathrm{T}}^{\mathrm{miss}})|$.
- $|\Delta\eta(\tau_1, \tau_2)|$: the absolute value of the difference of pseudorapidity between the two highest-p_{T} taus. A similar variable is also used for the $E_{\mathrm{T}}^{\mathrm{miss}}$ and taus, e.g. $|\Delta\eta(\tau, E_{\mathrm{T}}^{\mathrm{miss}})|$.

6 Direct stau production

The direct stau analysis targets the production of left- and/or right-handed staus, with the stau decaying to a τ and a $\tilde{\chi}_1^0$, as shown in Figure 1(a). This analysis aims to improve upon previous results, particularly for moderate mass splittings between the stau and $\tilde{\chi}_1^0$, and for $\tilde{\tau}_R\tilde{\tau}_R$ production. Multiple Boosted Decision Trees (BDTs) are trained for sensitivity to different areas of the $\tilde{\tau} - \tilde{\chi}_1^0$ phase space. The event selection and BDT training is described in Section 6.1, followed by the background estimation in Section 6.2.

6.1 Event selection

Events are selected using an asymmetric di-tau trigger: selected events for 2015–2017 (2018) datasets must have an offline τ candidate with $p_{\mathrm{T}} > 95$ GeV and a second τ candidate with $p_{\mathrm{T}} > 60$ (75) GeV, both matching the trigger signature.

Four BDTs are trained using the LightGBM [82] package on four groupings of signal scenarios chosen for their different $\tilde{\tau}$ masses and $\Delta m(\tilde{\tau}, \tilde{\chi}_1^0)$. Events used in training have at least two OS "medium" τ candidates, no electron, muon, or b-tagged jet candidates and pass loose selections on kinematic variables, as shown in Table 1. Three BDT SRs (SR-BDT1, SR-BDT2, SR-BDT3) have two bins in their BDT score, while the fourth BDT has only one bin (SR-BDT4) due to the low statistics available. The binned regions are used for setting exclusion limits in simplified models, while inclusive regions that merge the two bins in each SR are used to search for discoveries and to set model-independent limits. The events selected by the four BDT SRs significantly overlap, thus the SR with the best expected sensitivity will be chosen for interpretations.

The BDT training uses inputs including $E_{\mathrm{T}}^{\mathrm{miss}}$, the p_{T} and m_{T} of the two taus, $\Delta\phi$ between either τ and $E_{\mathrm{T}}^{\mathrm{miss}}$, $\Delta\eta(\tau_1, \tau_2)$ or $\Delta\eta(\tau, E_{\mathrm{T}}^{\mathrm{miss}})$, the invariant mass of the two τ candidates $m(\tau_1, \tau_2)$, m_{eff}, and m_{Tsum}. Cross Evaluation is used with three equal folds for a training, validation, and test set. To improve the reliability of the background modelling during training, input variables are pre-binned with bins defined such that the statistical error on the MC simulated background is less than 30% per bin. Futhermore, the maximum depth of the individual decision trees is restricted to one so that each tree makes only one selection on a variable. To avoid over-fitting, early-stopping is used, where trees cease to be added during training if performance on the relevant validation set does not improve after 10 trees. The fitting procedure is further constrained to avoid over-fitting by using regularization techniques, where BDT2 and BDT4 use

a higher amount of regularization than BDT1 and BDT3, and consequently, BDT2 and BDT4 occupy a smaller fraction of the total BDT score range compared to the others.

Table 1: Summary of the selection requirements for the stau pair production SRs.

	BDT Training Preselection			
	≥ 2 "medium" τ (OS) asymmetric di-tau Trigger e, μ, b-jet veto $E_{\mathrm{T}}^{\mathrm{miss}} > 20\,\mathrm{GeV}$ $m_{\mathrm{T2}} > 30\,\mathrm{GeV}$ $m(\tau_1, \tau_2) > 120\,\mathrm{GeV}$ $\Delta R(\tau_1, \tau_2) < 4$			
	SR-BDT1	SR-BDT2	SR-BDT3	SR-BDT4
Target scenario	Low $m_{\tilde{\tau}}$ Small $\Delta m(\tilde{\tau}, \tilde{\chi}_1^0)$	Mid $m_{\tilde{\tau}}$ Large $\Delta m(\tilde{\tau}, \tilde{\chi}_1^0)$	Mid $m_{\tilde{\tau}}$ Small $\Delta m(\tilde{\tau}, \tilde{\chi}_1^0)$	High $m_{\tilde{\tau}}$
	$= 2$ "medium" τ			
Bin 1	BDT1 score $\in (0.73, 0.78)$	BDT2 score $\in (0.78, 0.82)$	BDT3 score $\in (0.79, 0.86)$	BDT4 score > 0.64
Bin 2	BDT1 score > 0.78	BDT2 score > 0.82	BDT3 score > 0.86	–

6.2 Background estimation

The main backgrounds contributing to the direct stau SRs are from multi-jet production with misidentified taus, W and Z boson production in association with jets, multi-boson production, and events containing a top quark, referred to as *top* background. Top quark background events originate mostly from $t\bar{t}$ production in association with additional jets or an additional W or Z boson. The dominant SM backgrounds, W+jets, Z+jets, and top quark processes, are estimated using MC simulation normalised to data in dedicated control regions. The multi-jet background yield is estimated from data using an ABCD method, and MC simulation is used for all other SM backgrounds. The normalisation factors obtained from control regions are applied for backgrounds in the BDT training, as is the data driven multi-jet estimation.

6.2.1 Multi-jet background estimation

Background events contain a combination of 'real' taus, defined as correctly identified taus, or 'misidentified' taus, which can originate from a misidentified light-flavour quark or gluon jet, an electron, or a muon. Selected events from multi-jet production contain mostly misidentified taus originating from misidentified jets.

The multi-jet contribution is estimated from data using the so-called *ABCD* method, which is common to both the direct stau channel and the intermediate stau channel described in Section 7. All regions used for the ABCD method are schematically drawn in Figure 2. Four exclusive regions, labelled as A, B, C, and D, are defined in a two-dimensional plane as a function of two discriminating variables that are approximately uncorrelated. The number of multi-jet events in region D, N_{D}, can be calculated from that in region A, N_{A}, multiplied by the transfer factor $\mathrm{T} = N_{\mathrm{C}}/N_{\mathrm{B}}$. Region D corresponds to one of the SRs, whereas regions A, B, and C are control regions, thus regions A–D are labelled as CR-A, CR-B, CR-C, and SR-D. Furthermore, two validation regions, VR-E and VR-F, are defined to verify the reliability of the

transfer factor obtained from the ABCD estimation and to estimate the systematic uncertainty from the residual correlation between the variables used to define the ABCD regions. All of the regions are defined to be orthogonal to one another.

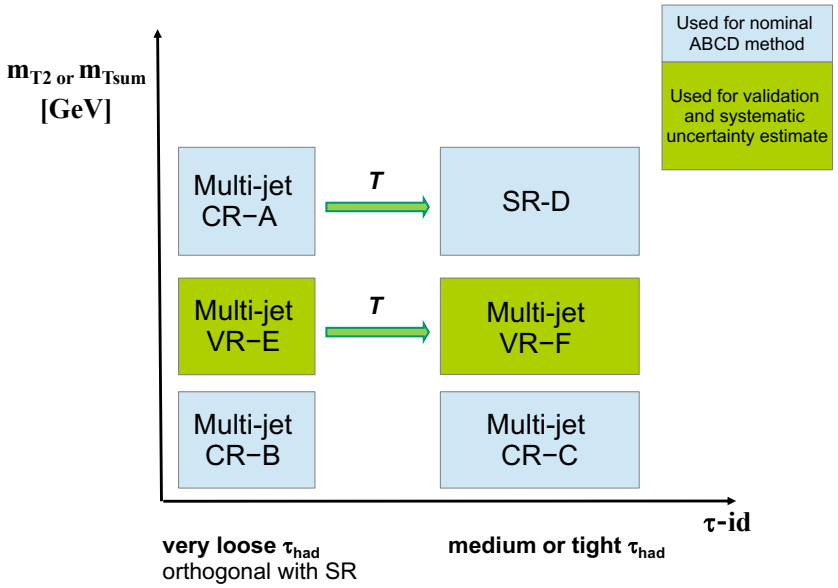

Figure 2: Illustration of the ABCD method for the multi-jet background determination. The control regions A, B, and C and signal region D are drawn as light blue boxes. Shown in green and labelled as VR are the regions E and F, which are used to validate the ABCD method and to estimate the systematic uncertainty.

A "very loose" τ identification criterion is used to define the regions CR-B, VR-E, and CR-A. To remain orthogonal to the requirements in SR-D, the two taus must be SS or not pass the "medium" criterion. Additionally, a requirement of $10 < m_{T2} < 20$ GeV is used to define control regions CR-B and CR-C, $20 < m_{T2} < 30$ GeV for VR-E and VR-F, while $m_{T2} > 30$ GeV is used for CR-A and SR-D. The tau p_T thresholds to ensure high triggering efficiency are not applied, effectively lowering the tau p_T thresholds to the online thresholds of 80 GeV and 50 GeV (60 GeV) for 2015–2017 (2018) data-taking. This increases statistics available and reduces the statistical uncertainty without affecting the transfer factor within uncertainties.

The number of multi-jet events in the control and validation regions is estimated from data after subtraction of other SM contributions estimated from MC simulation. In the case of the direct stau channel, the W+jets, Z+jets, and top quark backgrounds are subtracted after their normalisation to data in their dedicated CRs. Agreement between data and the estimated SM background is found in VR-E and VR-F, within statistical uncertainties.

A higher statistics validation region (MJVR) is also checked, with the same requirements as the direct stau SRs, but with low BDT scores (see Table 2). Good agreement is seen, as shown in Figure 3. The correlation between the τ identification and the kinematic variables is verified by studying the variation of the transfer factor as a function of the kinematic variables used and is found to be negligible.

The signal contamination in a certain region is defined as the ratio of the number of signal events to the sum of the number of signal events and SM background processes. The signal contamination in CRs and VRs is negligible for SUSY particle mass ranges not previously excluded by the ATLAS Collaboration.

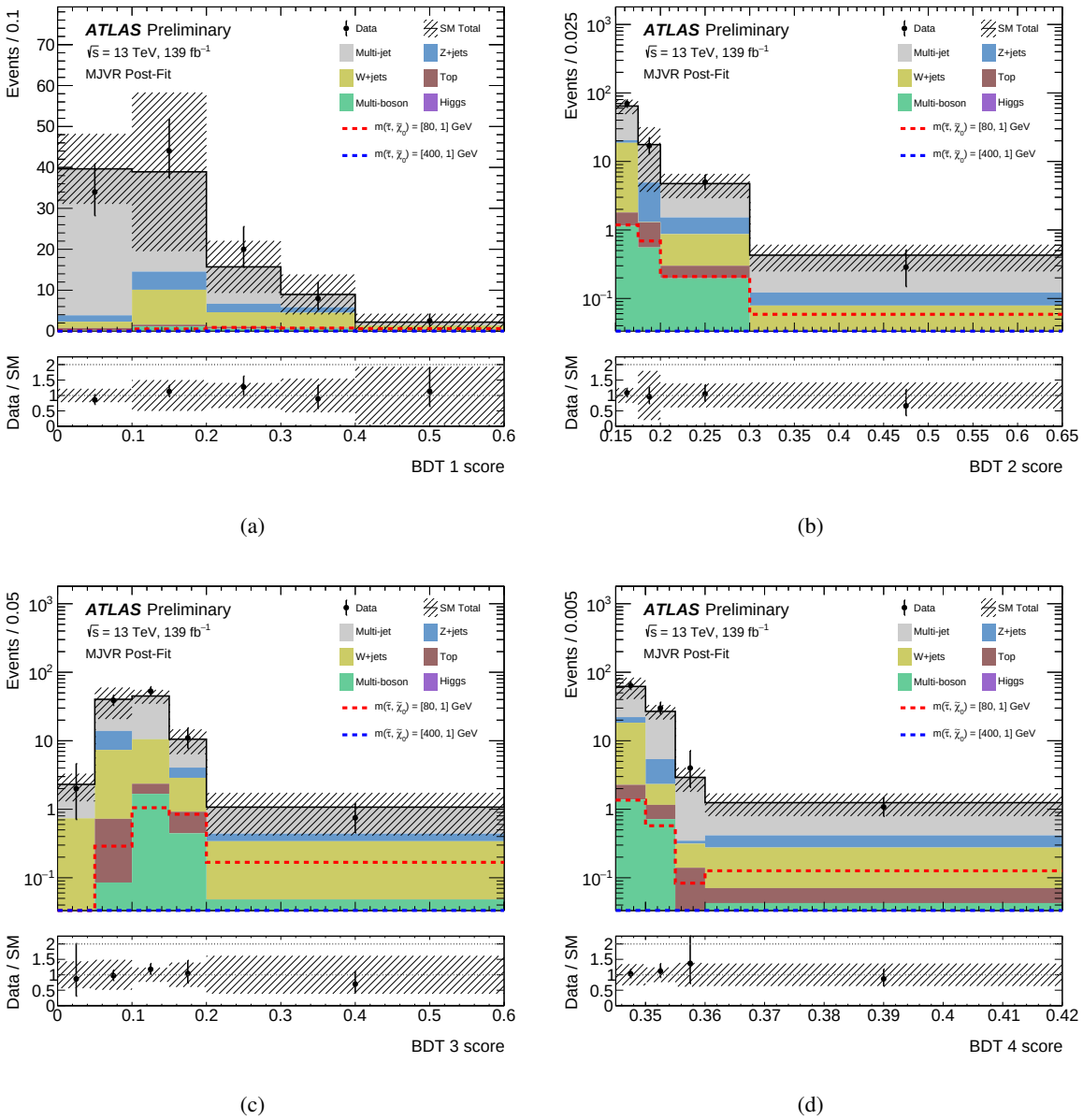

Figure 3: The post-fit BDT score distributions for the direct stau multi-jet background in MJVR, showing the scores for (a) BDT1, (b) BDT2, (c) BDT3, and (d) BDT4. A reduced range of BDT2 in (b) and BDT4 score in (d) are shown as they populate only a narrow range of the full score allowed. A few SUSY scenarios are overlaid for illustration. The hatched bands represent the combined statistical and systematic uncertainties of the total SM background. The lower panels show the ratio of data to the total SM background estimate.

Table 2: The definition of the control and validation regions for the direct stau channel.

Process	W+jets		Top	
Region	WCR	WVR	TCR	TVR
OS/SS	OS			
N "medium" τ	= 1		= 1	= 2
N e/μ	= 1 μ		= 1 μ	= 0
N b-jets	= 0		$\geq$ 1	$\geq$ 1
Trigger	single μ		single μ	asymm. di-tau
$p_{\mathrm{T}}(\tau_1)$ [GeV]	-		-	> 95
$p_{\mathrm{T}}(\tau_2)$ [GeV]	-		-	> 65
$\max[p_{\mathrm{T}}(\tau), p_{\mathrm{T}}(\mu)]$ [GeV]	> 95		> 95	-
$\min[p_{\mathrm{T}}(\tau), p_{\mathrm{T}}(\mu)]$ [GeV]	> 60		> 60	-
$E_{\mathrm{T}}^{\mathrm{miss}}$ [GeV]	> 20		> 20	-
$m_{\mathrm{T},\mu}$ [GeV]	$\in$ (50, 150]		$\in$ (50, 150]	-
m_{T2} [GeV]	> 30		> 30	
$m(\tau, \mu)$ [GeV]	> 120		> 120	–
$m(\tau_1, \tau_2)$ [GeV]	–		–	> 120
BDT score	All < 0.5	Any > 0.5	-	

Process	Z+jets		Multi-boson	Multi-jet	Inclusive
Region	ZCR	ZVR	MBVR	MJVR	InclVR
OS/SS	OS				
N "medium" τ	= 2		= 2	= 2	= 2
N e/μ	= 0		= 0	= 0	= 0
N b-jets	= 0		= 0	= 0	= 0
Trigger	asymm. di-tau		asymm. di-tau	asymm. di-tau	asymm. di-tau
$E_{\mathrm{T}}^{\mathrm{miss}}$ [GeV]	-		> 20	< 50	> 20
m_{T2} [GeV]	> 30		> 30	> 30	> 30
$m(\tau_1, \tau_2)$ [GeV]	< 120		< 120	> 120	> 120
$\Delta R(\tau_1, \tau_2)$	< 4		< 4	> 3	< 4
BDT score	BDT4 $\leq$ 0.60		BDT4 > 0.61	BDT1, BDT4 $\leq$ 0.60	
	BDT1 $\leq$ 0.10	BDT1 > 0.10		BDT2, BDT3 $\leq$ 0.70	

6.2.2 W+jets background estimation

The production of W+jets events with at least one misidentified τ is an important background, composing up to 50% of the expected SM background in the direct stau SRs. In order to correct the misidentified τ MC modelling and reduce theoretical uncertainty from W+jets background, dedicated control regions with W bosons decaying to $\mu\nu$ are used to select a pure WCR and normalise the W+jets MC estimate to data.

Events are required to pass a single-muon trigger using the lowest unprescaled p_{T} thresholds [83]. Events must contain exactly one isolated μ matching the trigger signature and one τ with the same charge selection as the signal regions. The contribution from events with top quarks is suppressed by rejecting events containing b-tagged jets. The contributions from Z+jets, top-quark and multi-boson production are reduced with m_{T} requirements.

In order to select events with kinematics similar to the SR definition, events with a small amount of $E_{\mathrm{T}}^{\mathrm{miss}}$ are removed and the charged leptons should pass p_{T} thresholds. Events in the WCR are selected by requiring all four BDT scores to be low, while the modelling is checked using a WVR with any one of the four BDT scores being high. The definitions of the WCR and WVR are given in Table 2. The purity of the selection in W+jets events is around 83% in the control and validation regions. The signal contamination in the WCR and WVR is negligible due to the requirement of an isolated muon in these regions.

6.2.3 Z+jets background estimation

The production of Z+jets where the Z boson decays to two taus is an irreducible background in the direct stau SRs, composing $7-50\%$ of the total SM background. The Z+jets background is estimated using MC simulation normalised to data in a control region, ZCR, which is similar to the SRs, but reverses the selection on $m(\tau_1, \tau_2)$. A low selection on the BDT4 score is made to avoid overlap with the validation region for multi-bosons (Section 6.2.5). A selection on the score for BDT1 is used to create an orthogonal validation region ZVR to check the modelling of the normalised Z+jets background. The definitions of the ZCR and ZVR are shown in Table 2.

6.2.4 Top quark background estimation

Events containing one or more top quarks also contribute significantly to the total background in the direct stau SRs at $7-30\%$. The Top quark background is estimated using MC simulation normalised to data in a control region, TCR, which, like the WCR, contains one isolated muon and one "medium" tau, but additionally requires a b-tagged jet. A validation region, TVR, is used to check the modelling of the Top quark background in events closer to the signal regions with two "medium" taus and a b-tagged jet. The definitions of the TCR and TVR are shown in Table 2.

6.2.5 Irreducible background estimation

Events with more than one SM W/Z boson are the dominant background in SR-BDT2 and SR-BDT4, with very small contributions from processes involving Higgs bosons in all SRs. These processes produce two real τ leptons and $E_{\mathrm{T}}^{\mathrm{miss}}$, and this irreducible background is taken from MC simulation. The modelling is checked using two validation regions. The first targets multi-boson production (MBVR) using a similar selection to SR-BDT4 but with the selection on $m(\tau_1, \tau_2)$ reversed. The second is a more inclusive validation region (InclVR) which checks the overall background estimation strategy and the modelling of the BDT score distributions. The definitions of these regions is shown in Table 2. The background estimation is seen to model the data well in these two regions and the agreement in the BDT score distributions in InclVR is shown in Figure 4.

Overall, the background estimation strategy is seen to model the data well in all validation regions used for the direct stau channel. The yields for the estimated SM background and data are shown in Figure 5 after the background-only fit to data has been applied, as described in Section 10.

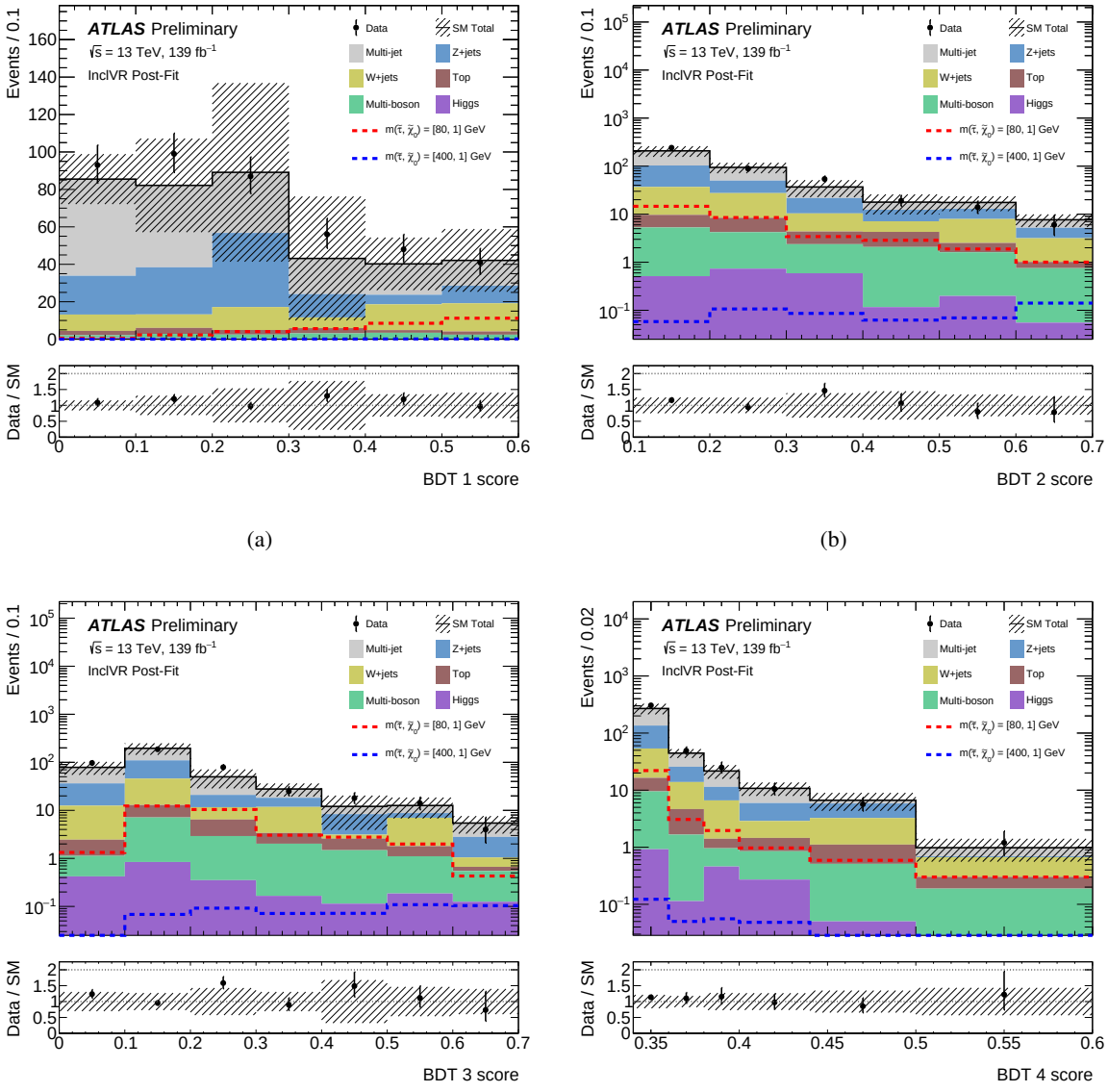

(a) (b)

(c) (d)

Figure 4: The post-fit BDT score distributions for the direct stau channel in InclVR, showing the scores for (a) BDT1, (b) BDT2, (c) BDT3, and (d) BDT4. A few SUSY scenarios are overlaid for illustration. The hatched bands represent the combined statistical and systematic uncertainties of the total SM background. Large uncertainties are seen in some bins due to a few highly weighted Z+jets MC simulation events migrating across bins when considering systematic variations. The lower panels show the ratio of data to the total SM background estimate.

7 Intermediate stau channel

The intermediate stau channel targets two different production mechanisms, $\tilde{\chi}_1^{\pm}\tilde{\chi}_2^0$ (C1N2) and $\tilde{\chi}_1^+\tilde{\chi}_1^-$ (C1C1), with decays to the lightest neutralino only through intermediate stau and tau sneutrinos, as shown in Figure 1(b) and Figure 1(c). The C1N2 analysis is then sub-divided into final states where the two

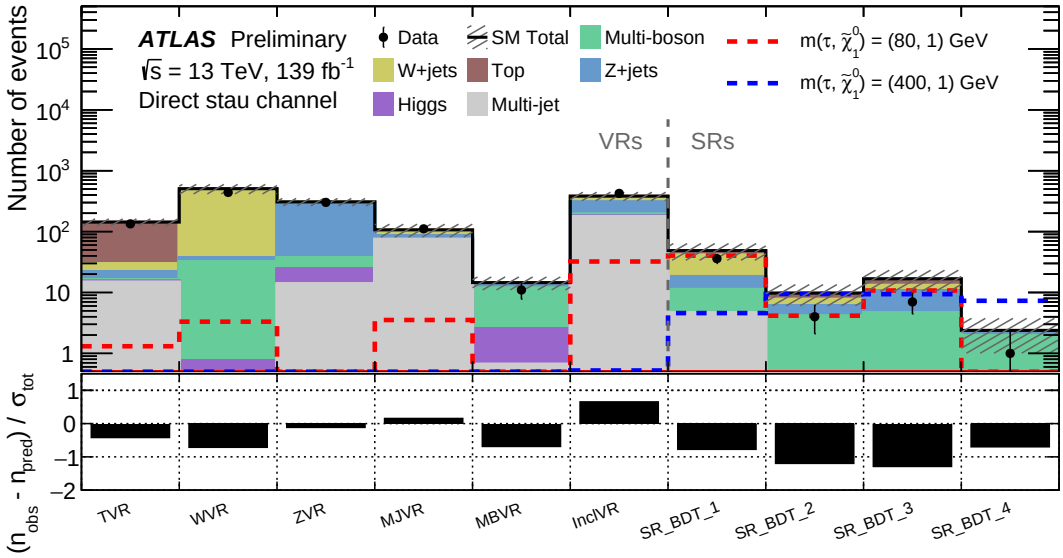

Figure 5: Comparison of the observed and expected event yields in all VRs and SRs after the background-only fit for the direct stau channel. A few SUSY scenarios are overlaid for illustration. The hatched band represents the combined statistical and systematic uncertainties of the total SM background. The lower panel shows the significance of any difference between the data and total SM background estimate yields.

highest-p_{T} τ candidates have opposite sign (OS) charge (C1N2OS) or have same sign (SS) charge, denoted as (C1N2SS). The SRs are separated into low mass (LM) and high mass (HM) regions to target respectively low or high $\tilde{\chi}_1^{\pm}/\tilde{\chi}_2^0$ mass regions. The high mass regions target the reach beyond the partial Run 2 dataset from the ATLAS collaboration, and the low mass regions target sensitivity in smaller mass splittings. The event selections of C1C1, C1N2OS and C1N2SS analyses are described in Section 7.1, and the background estimations are described in Section 7.2.

7.1 Event selection

The SRs were optimised by varying the kinematic selection criteria resulting in six SRs defined to cover both low mass (LM) and high mass (HM) regions for C1C1, C1N2OS and C1N2SS channels. The SRs were optimised to obtain the best expected sensitivity against the SM backgrounds. Events used in this channel must pass the same di-tau trigger described in Section 6.1, or a combined di-tau+$E_{\mathrm{T}}^{\mathrm{miss}}$ trigger. Events which pass the di-tau + $E_{\mathrm{T}}^{\mathrm{miss}}$ trigger for 2015–2017 (2018) datasets must have a τ candidate with $p_{\mathrm{T}} > 50\,(75)$ GeV, a second τ candidate with $p_{\mathrm{T}} > 40$ GeV (both matching the trigger signature), and the reconstructed $E_{\mathrm{T}}^{\mathrm{miss}} > 150$ GeV.

For the C1N2OS (C1N2SS) channels, events are required to have at least two "medium" τ candidates with OS (SS), while for the C1C1 channel, events are required to have exactly two "medium" τ candidates with OS. In the LM signal regions, SR-C1C1-LM and SR-C1N2OS-LM, at least one of the τ candidates must satisfy a tighter identification criteria, denoted as a "tight" τ candidate [76] to suppress quark or gluon jets misidentified as τ in the lower $E_{\mathrm{T}}^{\mathrm{miss}}$ region. Additionally, $E_{\mathrm{T}}^{\mathrm{miss}} > 60$ GeV is required in these two SRs to further suppress background from misidentified taus.

To discriminate the SUSY signal events from SM background processes, additional requirements are applied, as outlined in Table 3. Background processes producing τ pairs from low mass resonances, or from Z or Higgs bosons, are suppressed using high $m(\tau_1, \tau_2)$ selections, while top quark processes are suppressed with a b-jet veto. Contributions from $t\bar{t}$ and WW events are reduced using lower bounds on m_{T2} and m_{Tsum}.

Table 3: Summary of the selection requirements for the gaugino pair production SRs for channels that decay via an intermediate stau.

SR-C1C1-LM	SR-C1N2OS-LM	SR-C1N2SS-LM
= 2 "medium" τ (OS)	$\geq$ 2 "medium" τ (OS)	$\geq$ 2 "medium" τ (SS)
$\geq$ 1 "tight" τ		-
asymmetric di-tau trigger		
$E_{\mathrm{T}}^{\mathrm{miss}} < 150\,\mathrm{GeV}$		
b-jet veto		
-	$N_{\mathrm{jets}} < 3$	
$\lvert\Delta\phi(\tau_1, \tau_2)\rvert > 1.6$	-	$\lvert\Delta\phi(\tau_1, \tau_2)\rvert > 1.5$
Z/h veto ($m(\tau_1, \tau_2) > 120\,\mathrm{GeV}$)		-
$E_{\mathrm{T}}^{\mathrm{miss}} > 60\,\mathrm{GeV}$		$m_{\mathrm{Tsum}} > 200\,\mathrm{GeV}$
$m_{\mathrm{T2}} > 80\,\mathrm{GeV}$	$m_{\mathrm{T2}} > 70\,\mathrm{GeV}$	$m_{\mathrm{T2}} > 80\,\mathrm{GeV}$
SR-C1C1-HM	**SR-C1N2OS-HM**	**SR-C1N2SS-HM**
= 2 "medium" τ (OS)	$\geq$ 2 "medium" τ (OS)	$\geq$ 2 "medium" τ (SS)
di-tau + $E_{\mathrm{T}}^{\mathrm{miss}}$ trigger		
$E_{\mathrm{T}}^{\mathrm{miss}} > 150\,\mathrm{GeV}$		
b-jet veto		
Z/h veto ($m(\tau_1, \tau_2) > 120\,\mathrm{GeV}$)		-
$m_{\mathrm{Tsum}} > 400\,\mathrm{GeV}$		$m_{\mathrm{Tsum}} > 450\,\mathrm{GeV}$
$m_{\mathrm{T2}} > 85\,\mathrm{GeV}$		$m_{\mathrm{T2}} > 80\,\mathrm{GeV}$

7.2 Background estimation

The dominant backgrounds in the intermediate stau SRs are multi-jet production with misidentified taus, W+jets and Z+jets, multi-boson production, and top quark backgrounds. The multijet and W+jets backgrounds are estimated using the same methods described in Sections 6.2.1 and 6.2.2, respectively. The multi-jet background accounts for 28–48 % (<17 %) of the total SM yield in high mass SRs (low mass SRs) for all three scenarios, while W+jets accounts for 4–16 % of the total background. A dedicated CR is used to estimate the top quark backgrounds for the SS final state, where misidentified τ contributions are a dominant source, as described in Section 7.2.3.

Multi-boson production contributes mainly through events containing real taus resulting from WW and ZZ decaying into a $\tau\tau\nu\nu$ final state in C1C1 and C1N2OS scenarios, while in the C1N2SS scenario, the main process is WZ decaying into a $\tau\tau\tau\nu$ final state. The contribution from real taus exceeds 85-90% in Z+jets

and diboson production. Additionally, the real τ contribution exceeds 80% in backgrounds containing top quarks in OS final states. These backgrounds are described in Section 7.2.4.

7.2.1 Multi-jet background estimation

The same approach for the multi-jet backgroud estimation described in Section 6.2.1 is used for the intermediate stau channels, with the following changes as appropriate. The sign of the electric charge of the two taus (OS or SS), and m_{T2} and $\mathrm{m_{Tsum}}$ are used to define the control regions and validation regions, as shown in Table 4. In the C1C1 and C1N2OS scenarios, the m_{T2} variable is used to distinguish the regions of the ABCD method, while m_{Tsum} is used for the C1N2SS channel. In all validation regions and both sets of CR-B and CR-C, the events are required to pass a di-τ trigger, instead of the di-τ + $E_{\mathrm{T}}^{\mathrm{miss}}$ trigger in the intermediate stau channel to increase the statistics from the lower $E_{\mathrm{T}}^{\mathrm{miss}}$ requirements. The offline $E_{\mathrm{T}}^{\mathrm{miss}} > 150\,\mathrm{GeV}$ requirement is also removed. The di-τ trigger requires the identification of two hadronically decaying τ candidates with transverse momenta exceeding the same set of thresholds for the di-τ + $E_{\mathrm{T}}^{\mathrm{miss}}$ trigger, such that no bias on the taus is introduced.

Table 4: The definition of the ABCD regions for all channels in the intermediate stau scenarios. Only those requirements that differ between the CRs/VRs and the SRs are listed. A "very loose" τ identification criterion is used to define the regions CR-B, VR-E, and CR-A. The τ is also required to not pass the "medium" criterion to remain orthogonal to the requirements in SRs. The same τ identification criterion as that of the SR is used to define the regions CR-C and VR-F.

Channel	variable	CR-B / CR-C	VR-E / VR-F	CR-A / SR
C1C1-LM	m_{T2} [GeV]	$\in [15, 35]$	$\in [35, 80]$	> 80
	$E_{\mathrm{T}}^{\mathrm{miss}}$ [GeV]	$\in [10, 150]$	$\in [10, 150]$	$\in [60, 150]$
C1C1-HM	m_{T2} [GeV]	$\in [35, 60]$	$\in [60, 85]$	> 85
	m_{Tsum} [GeV]	$\in [100, 300]$	$\in [200, 400]$	> 400
	$E_{\mathrm{T}}^{\mathrm{miss}}$ [GeV]	> 50	> 50	> 150
C1N2OS-LM	m_{T2} [GeV]	$\in [15, 35]$	$\in [35, 70]$	> 70
	$E_{\mathrm{T}}^{\mathrm{miss}}$ [GeV]	$\in [10, 150]$	$\in [10, 150]$	$\in [60, 150]$
C1N2OS-HM	m_{T2} [GeV]	$\in [35, 60]$	$\in [60, 85]$	> 85
	m_{Tsum} [GeV]	$\in [150, 300]$	$\in [200, 400]$	> 400
	$E_{\mathrm{T}}^{\mathrm{miss}}$ [GeV]	> 50	> 50	> 150
C1N2SS-LM	m_{Tsum} [GeV]	< 100	$\in [100, 200]$	> 200
	$\lvert\Delta\phi(\tau_1, \tau_2)\rvert$	< 1.5	< 1.5	> 1.5
C1N2SS-HM	m_{Tsum} [GeV]	$\in [100, 200]$	$\in [200, 450]$	> 450
	$E_{\mathrm{T}}^{\mathrm{miss}}$ [GeV]	> 50	> 50	> 150

Agreement between data and the estimated SM background is found for the m_{T2} and m_{Tsum} distributions in the validation regions, as shown in Figure 6. Several signal reference points targeting sensitivity to LM and HM SRs are also shown to highlight the potential signal contamination in the VRs.

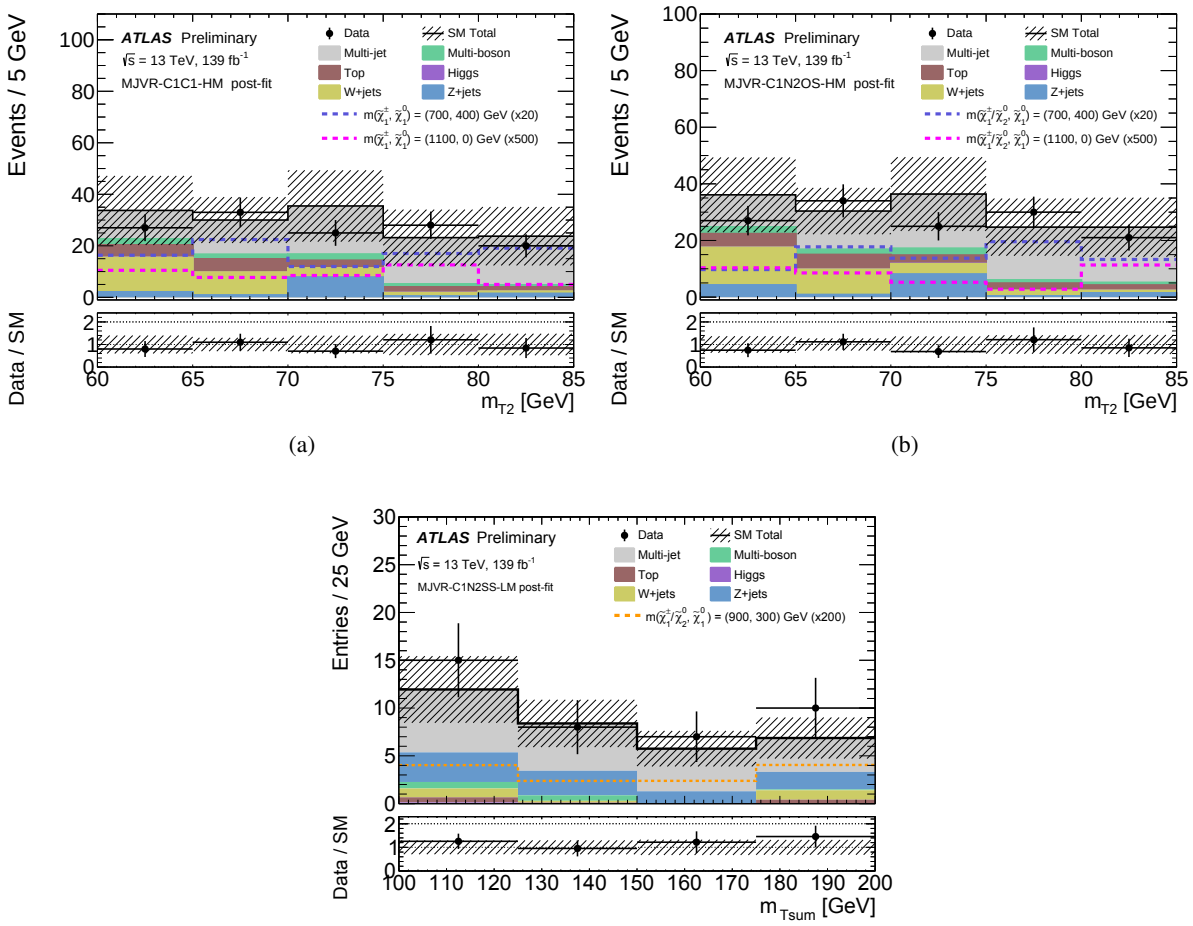

Figure 6: The post-fit kinematic distributions of m_{T2} and m_{Tsum} in the multi-jet background VR-F for (a) SR-C1C1-HM (MJVR-C1C1-HM), (b) SR-C1N2OS-HM (MJVR-C1N2OS-HM) and (c) SR-C1N2SS-LM (MJVR-C1N2SS-LM), respectively. A few SUSY scenarios are overlaid for illustration. The hatched bands represent the combined statistical and systematic uncertainties of the total SM background. The lower panels show the ratio of data to the total SM background estimate.

7.2.2 W+jets background estimation

The W+jets background is an important background for the intermediate stau channel. A similar approach as in Section 6.2.2 is used with the following modifications and the definitions for the WCRs and WVRs for OS/SS selections are shown in Table 5.

Top quark background events in the OS final state are labelled as "top-tagged" if they pass a dedicated selection; these events are vetoed in the WCR to suppress top quark background processes. Events are top-tagged using the contransverse mass variable [84], m_{CT}, to identify events that are kinematically compatible with $t\bar{t}$ pair production. Furthermore, top-tagged events must have at least two jets and the scalar sum of the p_{T} of at least one combination of two jets and the two leptons in the event must exceed 100 GeV. Contributions from Z+jets, top-quark and multi-boson production are reduced with selections on $m_{\mathrm{T},\mu}$ and $m_{\mathrm{T},\mu} + m_{\mathrm{T},\tau}$. The orthoganality of the WCRs and WVRs is ensured using $m_{\mathrm{T2}}(\tau, \mu)$ selections

and to select events with kinematics very similar to the SR definition, events with a small amount of $E_{\mathrm{T}}^{\mathrm{miss}}$ are removed. The purity of the selection in W+jets events is 73–85 % in all W control and validation regions. The signal contamination in the WCR and WVR is negligible due to the requirement of a muon in the event.

The multi-jet contribution in the WCR (WVR) is estimated using the so-called OS–SS method by counting the number of events in data satisfying the same requirements as the WCR (WVR) but requiring the electric charge of the two leptons to be different from that in the SRs. Event yields from SM processes other than multi-jet production are subtracted from the data in the WCR, leaving only the events for the multi-jet estimate. The OS–SS method relies on the fact that in the multi-jet background, the ratio of SS to OS events is close to unity, while a significant difference from unity is expected for W+jets production. The latter is dominated by gu/gd-initiated processes that often give rise to a jet originating from a quark, the charge of which is anti-correlated with the W-boson charge. Based on studies with simulated samples, a conservative systematic uncertainty of 100 % is assigned to the estimate of the multi-jet event yield in the WCR.

Table 5: The definition of the W+jets and Top quark control and validation regions for the intermediate stau channel.

Process	W+jets				Top	
Region	WCR-OS	WVR-OS	WCR-SS	WVR-SS	TCR-SS-HM	TVR-SS-HM
OS/SS	OS		SS		SS	
N "medium" τ	= 1				< 2	
N "loose" τ	-				≥ 2 "very loose", ≥ 1 "loose"	
N e/μ	= 1 μ				-	
N b-jets	= 0				≥ 1	
Trigger	single μ				di-τ + $E_{\mathrm{T}}^{\mathrm{miss}}$	
$p_{\mathrm{T}}(\tau)$ [GeV]	> 50				-	
$p_{\mathrm{T}}(\mu)$ [GeV]	> 40				-	
Top tagged	veto		-		-	
$m_{\mathrm{T},\mu}$ [GeV]	< 140		∈ (50, 150]		-	
$m_{\mathrm{T},\mu} + m_{\mathrm{T},\tau}$ [GeV]	-		> 80		-	
$E_{\mathrm{T}}^{\mathrm{miss}}$ [GeV]	> 60		> 50		> 150	
m_{T2} [GeV]	∈ (40, 70]	> 70	< 60	> 60	-	
m_{Tsum} [GeV]	-		-		< 400	> 400

7.2.3 Top quark background estimation for C1N2SS

The top quark background in SR-C1N2SS-LM is very small (<1%) and mostly composed of two real taus, and so is estimated with MC simulation. However, the top quark background is a dominant contribution in SR-C1N2SS-HM and mostly consists of one or two misidentified taus from $t\bar{t}$ and Wt production. To estimate this background in SR-C1N2SS-HM, a data-driven approach is used to normalise the top quark background MC simulation to data using a dedicated top-enriched CR (TCR-SS-HM) and validated in a top-enriched VR (TVR-SS-HM), described in Table 5. The τ identification working point was loosened to increase the statistics in these regions, while high $E_{\mathrm{T}}^{\mathrm{miss}}$ is required to suppress the contribution from multi-jet processes. The top quark background purity in the top quark CR and VR for SR-C1N2SS-HM (TCR-SS-HM and TVR-SS-HM) is high at >83%.

7.2.4 Irreducible background estimation

Additional irreducible SM backgrounds are estimated from MC simulation and checked in dedicated VRs. The top quark background contributions in OS final states are small and amount to about 7–14 % of the total background in all SRs. Two regions enriched in top-quark events are defined to validate the top quark modelling in OS events, TVR-OS-LM and TVR-OS-HM for the low and high mass SR kinematics, respectively. At least two "medium" taus are required, in which at least one τ candidate must satisfy the "tight" τ identification criteria. To be orthogonal with the SRs and increase the contribution from top quark events, one b-tagged jet with $p_{\mathrm{T}} > 20\,\mathrm{GeV}$ is required, while $|\Delta\phi(\tau_1, \tau_2)| > 1.0$ and $E_{\mathrm{T}}^{\mathrm{miss}} > 20\,\mathrm{GeV}$ are used to suppress the Z+jets background. The Z+jets and Higgs boson backgrounds are further reduced using $m(\tau_1, \tau_2) > 120\,\mathrm{GeV}$. Finally, other SM background contributions are suppressed by requiring $m_{\mathrm{Tsum}} > 150\,\mathrm{GeV}$ and $\mathrm{m_{T2}} > 40\,(30)\,\mathrm{GeV}$ in TVR-OS-LM (TVR-OS-HM).

The Z+jets contribution is 16–21 % of the total background in all OS SRs and mainly arises from $Z \to \tau\tau$ decays. The multi-boson background accounts for 25–50 % of the total SM contribution in the SRs and mainly arises from $WW \to \tau\nu\tau\nu$ and $ZZ \to \tau\tau\nu\nu$ events. The purity of real taus is typically above 96 %.

To validate the MC modelling and normalisation of the Z+jets and multi-boson processes, four dedicated VRs are defined: ZVR-OS-LM (MBVR-OS-LM) is defined to validate Z+jets (multi-boson) MC modelling in the low mass SRs, while ZVR-OS-HM (MBVR-OS-HM) is defined to validate the MC modelling in the high mass SRs. At least two "medium" taus are required and to suppress top-quark backgrounds, events containing b-jets are vetoed. A selection on $E_{\mathrm{T}}^{\mathrm{miss}}$ of 40 (70) GeV is required in ZVR-OS-LM (MBVR-OS-LM), and requirements on $|\Delta R(\tau_1, \tau_2)| < 1.0$ ($|\Delta R(\tau_1, \tau_2)| < 1.2$ and $|\Delta\phi(\tau_1, \tau_2)| < 1.0$) are used to suppress other SM backgrounds in Z+jets (multi-boson) VRs. In the MBVRs, $m_{\mathrm{T},\tau 1} + m_{\mathrm{T},\tau 2} > 180\,\mathrm{GeV}$ is also required to enrich the multi-boson contribution and suppress the Z+jets events. Finally, the ZVRs and MBVRs are separated by an m_{T2} requirement at 60 GeV to keep them orthogonal and further increase their purity.

The purity of the selection in $t\bar{t}$ and Z+jets events is in the range of 81–99 % in the respective validation regions, and the purity of the selection in multi-boson events is 41–68 % in the MBVRs. The signal contamination in the above VRs is small due to the b-jet requirement in the top-quark VRs and the $m(\tau_1, \tau_2)$ upper thresholds in the Z+jets and multi-boson VRs.

In the SS final state, the multi-boson background is estimated from MC simulation and validated in a dedicated VR (MBVR-SS). Events must have two isolated muons with OS, pass the single muon trigger, and have no b-tagged jets to suppress top quark contribution. To enrich multi-boson production, $|\Delta\phi(\tau, E_T^{\mathrm{miss}})| < 1.75$ and $E_{\mathrm{T}}^{\mathrm{miss}} > 100\,\mathrm{GeV}$ requirements are applied, resulting in a multi-boson purity of 73%.

The agreement between data and the SM prediction is shown in all validation and signal regions for the intermediate stau channels in Figure 7 after the background-only fit to data has been applied, as described in Section 10.

8 Intermediate Wh channel

The search for the production of $\tilde{\chi}_1^{\pm}\tilde{\chi}_2^0$ decaying via an intermediate W and h boson, as shown in Figure 1(d), is described in this section. The analysis targets the leptonic decay of the W boson to an electron or muon,

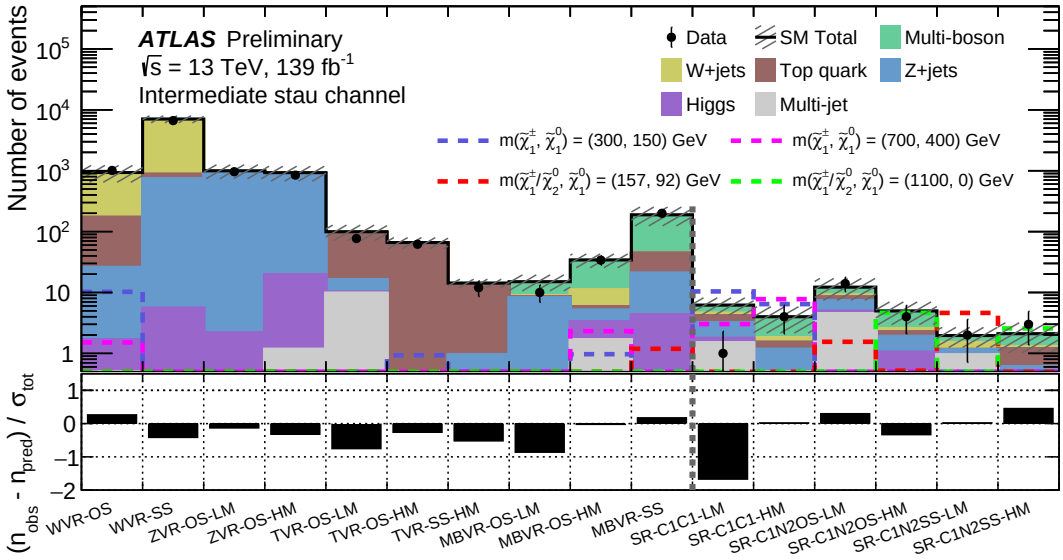

Figure 7: Comparison of the observed and expected event yields in all VRs and SRs after the background-only fit for the signal regions targeting chargino/neutralino production and decay via intermediate staus. A few SUSY scenarios are overlaid for illustration. The hatched band represents the combined statistical and systematic uncertainties of the total SM background. The lower panel shows the significance of any difference between the data and total SM background estimate yields.

and the decay of the Higgs boson to two OS taus. The event selection of the intermediate Wh channel is described in Section 8.1 and the background estimations are described in Section 8.2.

8.1 Event selection

Events for the intermediate Wh channel must have at least two hadronically decaying taus with OS and exactly one light lepton (e or μ). The selected light lepton must pass the signal electron or muon requirements described in Section 4 and also pass the unprescaled single electron or single muon trigger with an offline threshold of $p_{\mathrm{T}} > 27$GeV. Two SRs are defined to cover low mass (SR-Wh-LM) and high mass (SR-Wh-HM) $\tilde{\chi}_1^{\pm}\tilde{\chi}_2^0$ production, with an overlapping selection, as shown in Table 6. The invariant mass of the two taus, $m(\tau_1, \tau_2)$, is required to be compatible with the Higgs boson mass, while the b-jet veto and $|\Delta R(\tau_1, \tau_2)|$ requirements suppress the top quark and fake τ backgrounds, respectively. High m_{T2}, $m_{\mathrm{T},\ell}$ and $m_{\mathrm{T}sum}$ requirements provide good discrimination between SUSY signal events and SM background.

8.2 Background estimation

The SM backgrounds for a final state with two hadronically decaying taus from a Higgs boson decay and one light lepton from a W-boson decay can be separated into two groups. The first group is composed of events with a real light lepton and two real taus, and is dominated by multi-boson processes which are estimated using MC simulation. The second group includes processes with one or two taus from misidentified jets. Events with a single misidentified τ are dominated by events with a top quark, which is estimated using

Table 6: Summary of selection requirements for the SRs of gaugino pair production decaying to an intermediate Wh for low mass and high mass regions. The two SRs are not orthogonal.

SR-Wh-LM	SR-Wh-HM
= 1 light lepton	
≥ 2 "medium" τ (OS)	
b-jet veto	
$\lvert\Delta\phi(\tau_1,\tau_2)\rvert < 3$	
-	$\Delta R(\tau_1,\tau_2) < 2.2$
$90 < m(\tau_1,\tau_2) < 130\,\text{GeV}$	$80 < m(\tau_1,\tau_2) < 160\,\text{GeV}$
$m_{T2} > 100\,\text{GeV}$	$m_{T2} > 80\,\text{GeV}$
-	$m_{T,\ell} > 80\,\text{GeV}$
-	$m_{Tsum} > 450\,\text{GeV}$

MC normalised to data in a dedicated CR. Events with two misidentified taus are mostly from W+jets events and are estimated using a data-driven technique – the fake factor method. All other SM backgrounds are estimated directly from MC simulation. Overall, the dominant background contributions in both SRs are from top quark and multi-boson processes, and account for 89–90% of the total background.

8.2.1 Misidentified τ background estimation

The W+jets process dominates the background with two misidentified taus, with less than 6–7 % contribution from other processes. The fake factor method estimates all processes with two misidentified taus using a control data sample (FFCR) with taus that fail the nominal τ identification requirement. This estimate is obtained as the product of the number of FFCR events and the fake factor, which relates the number of events with looser tau-lepton candidates to the number where tau leptons meet the nominal identification criteria.

To compute the fake factor (FF), a looser set of criteria for the τ identification is used, providing a selection orthogonal to the default τ selection – the control sample is referred to as the anti-τ sample. The FF value for each of the τ candidates is the ratio of the number of events with a τ passing the identification requirements to the number passing the anti-τ selection requirements. To estimate the two misidentified τ contributions, three control regions are defined using the identification criteria of the two highest-p_{T} taus: one region where both candidates satisfy the anti-τ criteria ("AA" region), one region where the first candidate passes the "medium" identification criteria and the second candidate satisfies the anti-τ criteria ("MA" region), and one region where both candidates pass the "medium" identification criteria ("MM" region). In this case, the fake factor extrapolation to the SR is derived for the highest-p_{T} τ candidate first, then the second highest-p_{T} τ candidate.

The estimation of the contribution from processes with two misidentified taus (N_{fakes}) can be written as the product of the two fake factors ($\text{FF}_{\tau i}^{\text{CR}}$) and the number of events from the "AA" region ($N_{\text{AA, fake bkg}}$):

$$N_{\text{fakes}} = N_{\text{AA, fakes}} \times \text{FF}_{\tau 1}^{\text{CR}} \times \text{FF}_{\tau 2}^{\text{CR}}, \tag{1}$$

where the individual fake factors for the two taus are written as:

$$\text{FF}_{\tau 1}^{\text{CR}} = \frac{N_{\text{data,AA}} - N_{\text{MC,AA}}^{\geq 1 \text{ truth } \tau}}{N_{\text{data,MA}} - N_{\text{MC,MA}}^{\geq 1 \text{ truth } \tau}} \tag{2}$$

$$\mathrm{FF}_{\tau 2}^{\mathrm{CR}} = \frac{N_{\mathrm{data,MA}} - N_{\mathrm{MC,MA}}^{\geq 1 \text{ truth } \tau}}{N_{\mathrm{data,MM}} - N_{\mathrm{MC,MM}}^{\geq 1 \text{ truth } \tau}} \,. \tag{3}$$

The contamination from events with at least one real τ ($N_{\mathrm{MC}}^{\geq 1 \text{ truth tau}}$) is estimated from MC simulation and subtracted when calculating the ratio.

The fake factors are calculated in a W-enriched control region (FFCR-Wh), which maximises available statistics by loosening kinematic selection requirements and remains orthogonal to the SRs by inverting the OS requirement, as summarised in Table 7.

Table 7: The definition of the fake factor control and validation regions, FFCR-Wh and FFVR-Wh, respectively.

FFCR-Wh	FFVR-Wh
≥ 2 "very loose" τ (SS)	≥ 2 "medium" τ (OS)
=1 light lepton (e or μ)	
b-jet veto	
$\lvert\Delta\phi(\tau_1,\tau_2)\rvert < 3$	
$m(\tau_1,\tau_2) > 20\,\mathrm{GeV}$	$40 < m(\tau_1,\tau_2) < 160\,\mathrm{GeV}$
$m_{\mathrm{T2}} > 20\,\mathrm{GeV}$	$m_{\mathrm{T2}} > 30\,\mathrm{GeV}$

The fake factor dependencies on the parameters of the τ candidates, such as the number of tracks, p_{T} and $|\eta|$, have been studied and are found to be minimal except for the number of tracks (1-prong or 3-prong taus). The fake factors are measured in bins of p_{T} and $|\eta|$, separately for 1-prong and 3-prong taus, with the binning optimised based on the available statistics. The fake factor for the two highest-p_{T} taus is similar at around 0.4 (0.1) for the 1-prong (3-prong) taus. The fake factor estimation is validated in a misidentified τ dominated VR (FFVR-Wh) with a selection similar to the SR-Wh-LM with loosened selections on $m(\tau_1,\tau_2)$ and m_{T2}, as shown in Table 7. The kinematic distributions in FFVR-Wh are shown in Figure 8 and good agreement between data and SM prediction is observed.

8.2.2 Top quark background estimation

The top quark background is small in SR-Wh-HM and is accounted for in the estimation with the FF method since it is dominated by two misidentified taus. However, in SR-Wh-LM the top quark background is more important and is comprised mainly of $t\bar{t}$ events with one W-boson decay to an electron or muon, and the other to a τ – the second τ typically originates from a misidentified jet. The top quark background is estimated from MC and normalised to data using a top quark enriched control region (TCR-Wh) and validated in a top-quark VR (TVR-Wh), as defined in Table 8. MC simulation shows the top quark background composition is similar across the CR, VR and SR. The selection for the control and validation region are similar to the SR selection, but with one or two b-jets required to be orthogonal to the SR. To increase the statistics, the OS requirement is removed and the $m(\tau_1,\tau_2)$ requirement is also loosened, and to improve the purity of the top quark background, high $m_{\mathrm{T}sum}$ is required. The top quark background purity is between 73–81% in the CR and VR.

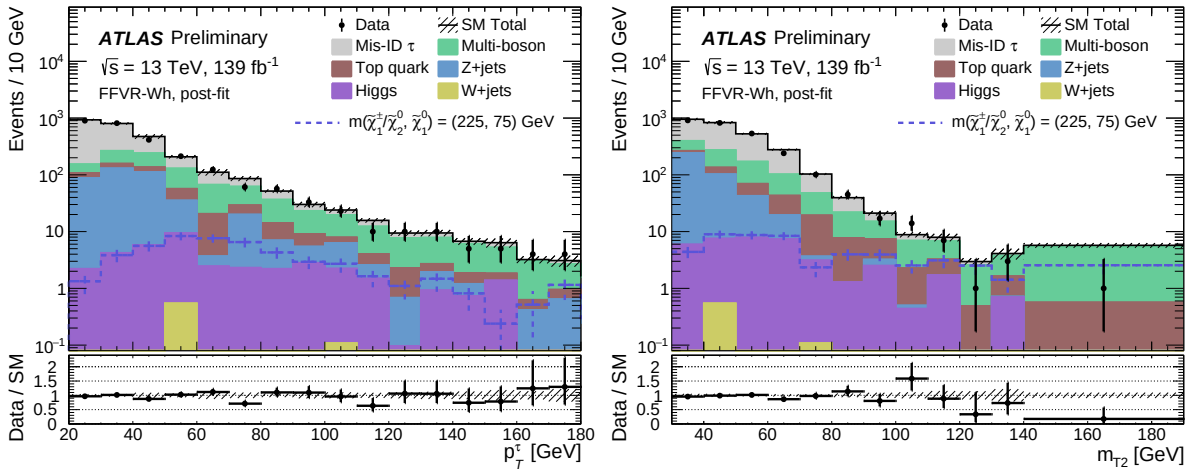

(a) (b)

Figure 8: The post-fit distributions of (a) the highest-p_{T} τ transverse momentum p_{T}^{τ} and (b) m_{T2} variables in FFVR-Wh. The misidentified contribution with at least two misidentified taus (Mis-ID τ) is estimated from data using the fake factor method. A few SUSY scenarios are overlaid for illustration. The hatched bands represent the combined statistical and systematic uncertainties of the total SM background. The lower panels show the ratio of data to the total SM background estimate.

Table 8: The definition of the top quark and multi-boson control and validation regions for the intermediate Wh channel.

Process	Top		Multi-boson
Region	TCR-Wh	TVR-Wh	MBVR-Wh
OS/SS	OS		
N "medium" τ	≥ 2		
N e/μ	$= 1$ e/μ		
Trigger	single e/μ		
$\lvert\Delta\phi(\tau_1,\tau_2)\rvert$	< 3		
N b-jets	$\in [1,2]$		$= 0$
$p_{T\tau_2}$ [GeV]	-		> 30
$m_{\mathrm{T},l}$ [GeV]	-		> 70
$m(\tau_1,\tau_2)$ [GeV]	$\in (40,160]$		$\in (40,70]$
$m_{\mathrm{T}sum}$ [GeV]	> 250		-
m_{T2} [GeV]	$\in (20,80]$	> 80	< 80

8.2.3 Multi-boson background estimation

Multi-boson production is the dominant SM contribution in both intermediate Wh SRs. The main contribution is WZ production with both bosons decaying leptonically, giving one light lepton and two real taus in both SRs. Smaller contributions in SR-Wh-LM stem from ZZ or WW production decaying to one light lepton, one real τ, and one misidentified τ.

The multi-boson background is estimated from MC simulation and validated in a multi-boson enriched region, MBVR-Wh, defined in Table 8. Compared to the SRs, the selection on the invariant mass of the taus is lowered and an upper threshold on m_{T2} of 80 GeV is required. The multi-boson purity is found to be 61% in MBVR-Wh. The agreement between data and the SM prediction is shown in the validation and signal regions for the intermediate Wh channels in Figure 9.

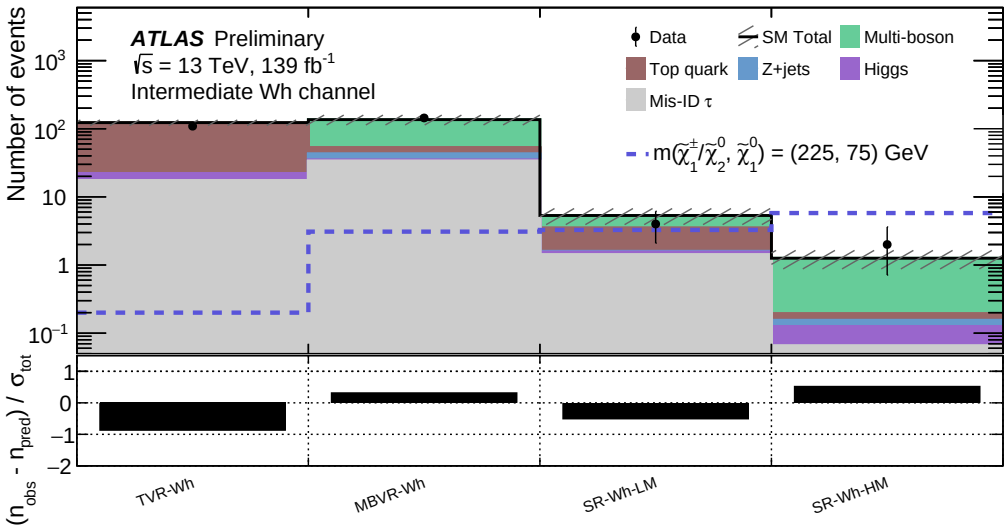

Figure 9: Comparison of the observed and expected event yields in the TVRs and MBVRs as well as two SRs after the background-only fit. A few SUSY scenarios are overlaid for illustration. The hatched band represents the combined statistical and systematic uncertainties of the total SM background. The lower panel shows the significance of any difference between the data and total SM background estimate yields.

9 Systematic uncertainties

Systematic uncertainties have an impact on the background and signal estimates in the control and signal regions. Uncertainties arising from experimental effects and theoretical sources are considered. The main sources of experimental systematic uncertainty in the SM background estimates include τ and jet-energy calibrations and resolution, τ identification, systematic effects due to the presence of pile-up events, and uncertainties related to the modelling of $E_{\mathrm{T}}^{\mathrm{miss}}$ in the simulation. The uncertainties in the energy and momentum scale of each of the objects entering the $E_{\mathrm{T}}^{\mathrm{miss}}$ calculation are estimated, as well as the uncertainties in the soft-term resolution and scale [85]. A variation in the pile-up reweighting of the MC simulated event samples is included to cover the uncertainty in the ratio of the predicted and measured inelastic cross-section [86]. The uncertainty on the combined 2015–2018 integrated luminosity

was measured to be 1.7% [87], obtained using the LUCID-2 detector [88] for the primary luminosity measurements.

Theoretical uncertainties affecting the main irreducible backgrounds W+jets, Z+jets, top quark processes, and dibosons, are estimated by varying the generator parameters: renormalisation and factorisation scale as well as PDF uncertainties following the PDF4LHC recommendations [89]. Uncertainties due to the choice of renormalisation and factorisation scales are included by varying the scales from their nominal values by a factor of two or one half – the two scale variations are taken as uncorrelated and the additional coherent up/down variation of the two scales is also considered. Additionally, cross-section uncertainties are assigned to be included in the normalisation of the signal and the background processes taken directly from MC simulation.

Several sources of uncertainty are considered for the ABCD method used to determine the multi-jet background estimation for direct stau production and the intermediate stau channel, they include: the correlation between the τ identification and the kinematic variables m_{T2}, the limited number of events in the CRs, and the subtraction of other SM backgrounds. The systematic uncertainty in the correlation is estimated by comparing the transfer factor from CR-B to CR-C to that of VR-E to VR-F. The systematic uncertainty in the non-multi-jet background subtraction in the control regions is estimated by considering the total uncertainties of the MC estimates of the non-multi-jet background in the CRs. The systematic uncertainty due to the limited number of events in the control regions is estimated by taking the statistical uncertainty of the event yields in these control regions.

Sources of uncertainty are considered for the fake factor method used to determine the misidentified background with at least two misidentified taus in the intermediate Wh channel. The fake factor values are varied up and down by their statistical uncertainties and the difference is used as a source of uncertainty. A further 30% systematic uncertainty on the subtracted MC processes is used as a conservative estimation on the systematic uncertainty from MC subtractions in the FFCR-Wh. The difference in the quark/gluon contributions in the fake factor control regions and signal regions was studied and found to be negligible compared to the uncertainties placed on the overall normalisation and statistical contributions. The systematic uncertainties and their impact on each SR is summarised in Figure 10.

The dominant contribution of systematic uncertainties in all scenarios are mainly from the statistics of the MC samples, the normalisation uncertainties of the multi-jet background, the τ identification and the energy scale, jet energy scale and resolution. In the intermediate stau channel, uncertainties on the multi-jet estimation are also important. In the direct stau and intermediate Wh channels, multi-boson theory uncertainties represent a major contribution to the systematics.

10 Results

The observed number of events in the CRs and SRs are used in a combined profile likelihood fit to determine the expected SM background yields. The statistical interpretation of the results is performed using the profile likelihood method implemented in the HistFitter framework [90]. Systematic uncertainties are included as nuisance parameters in the likelihood fits and are assumed to follow a Gaussian distribution with a width determined from the size of the uncertainty. Correlations of systematic uncertainties between control and signal regions, and between background processes are taken into account with common nuisance parameters. The fit parameters are determined by maximising the product of the Poisson probability functions and the constraints for the nuisance parameters.

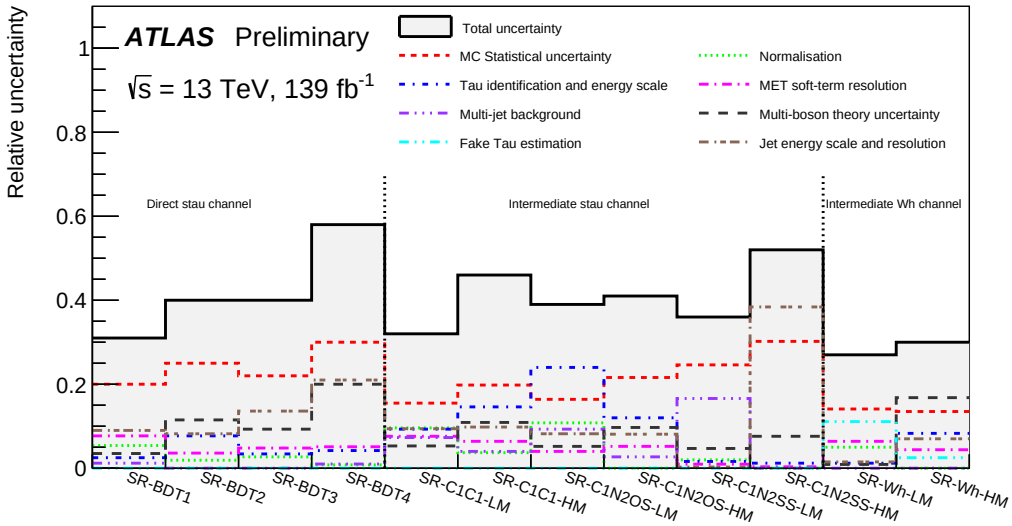

Figure 10: Summary of the total uncertainty on the predictions of the background event yields of each SR in the three search channels. The dominant systematic contributions are indicated by individual dashed lines. The total uncertainty in each SR is denoted by the solid black line.

To constrain the SM backgrounds normalised to data in CRs, the *background-only* fit is used. This uses the observed yields in the CRs with the expected SM contributions (other than multi-jet) in the CRs and SRs, as well as the corresponding background transfer factors. The free parameters in the fit are the normalisations of the SM processes and no BSM signal is assumed. To estimate the SM background in the SRs, the observed data in the SRs is also included and a combined fit is performed, taking into account any correlations between CRs and SRs, as well as between background processes. To assess the possibility of the presence of BSM events in signal regions, the *model-independent* fit is used. This uses the observed yields in both the CRs and SRs with the SM background estimates to test whether any BSM events could be present in the SR. The significance of a possible excess of observed events over the SM prediction is quantified by the one-sided probability, $p(\text{signal} = 0)$ denoted by p_0, of the background alone to fluctuate to the observed number of events or higher using the asymptotic formula described in Ref. [91]. The upper limit on the visible cross-section of BSM events in a SR, σ^{95}_{vis}, is also calculated, which includes the acceptance and efficiency effect of any BSM signal possibly present. Finally, to assess the compatibility of the signal scenarios with the data observation, the *model-dependent* fit is used, which accounts for the SUSY signal in all CRs and SRs scaled by a floating signal normalisation factor. The background normalisation factors are also determined simultaneously in the fit. A SUSY scenario is rejected if the upper limit at 95 % confidence level (CL) of the signal normalisation factor obtained in this fit is smaller than the predicted cross-section of the scenario [92].

10.1 Direct stau production analysis

The expected and observed numbers of events in the direct stau signal regions are shown in Table 9, where the observations are consistent with the SM expectations. All the SR-BDT strongly overlap and show a common deficit of significance $0.7 - 1.3\,\sigma$. For example, the single event in data selected by SR-BDT4 is also selected by the other three SR-BDT, while the four events in SR-BDT2 are also selected by SR-BDT3.

The W+jets, Z+jets, and top quark backgrounds are normalised to data in their respective control regions, obtaining normalisation factors of 0.93 ± 0.11, 0.91 ± 0.07, and 0.85 ± 0.05, respectively, as shown in Table 10.

Table 9: Observed and expected numbers of events after the background-only fit in the signal regions targeting direct stau production. The uncertainties correspond to the sum of statistical and systematic uncertainties. The correlation of systematic uncertainties among control regions and among background processes is taken into account. The one-sided p_0-value, and the observed and expected 95 % CL upper limits on the visible non-SM cross-section (σ_{vis}^{95}) from the model-independent fit are given for the unbinned SRs. Values of $p_0 > 0.5$ are truncated to $p_0 = 0.5$

SM process	SR-BDT1	SR-BDT1_bin0	SR-BDT1_bin1	SR-BDT2	SR-BDT2_bin0	SR-BDT2_bin1
Multi-boson	6.6 ± 2.9	3.3 ± 1.7	3.3 ± 1.7	4.1 ± 1.9	1.7 ± 1.0	2.3 ± 1.1
W+jets	23 ± 9	12 ± 6	11 ± 4	$1.6^{+1.7}_{-1.6}$	$1.5^{+1.6}_{-1.5}$	$0.1^{+0.1}_{-0.1}$
Top quark	7.8 ± 2.5	3.3 ± 1.6	4.5 ± 1.9	2.1 ± 1.2	1.0 ± 1.0	1.0 ± 0.7
Z+jets	7 ± 6	4 ± 4	2.8 ± 2.3	2.0 ± 1.1	1.6 ± 0.9	0.4 ± 0.2
Higgs	0.01 ± 0.01	$0.0^{+0.0}_{-0.0}$	$0.0^{+0.0}_{-0.0}$	$0.02^{+0.12}_{-0.02}$	$0.0^{+0.1}_{-0.0}$	0.0 ± 0.0
Multi-jet	4.6 ± 1.2	2.2 ± 0.8	2.4 ± 0.7	0.02 ± 0.00	0.0 ± 0.0	0.0 ± 0.0
SM total	49 ± 15	25 ± 10	24 ± 8	10 ± 4	5.9 ± 3.1	3.9 ± 1.5
Observed	36	22	14	4	3	1
$m(\tilde{\tau}, \tilde{\chi}_1^0) = (80, 1)$ GeV	40.3 ± 1.4	13.6 ± 0.8	26.7 ± 1.1	4.2 ± 0.4	3.4 ± 0.4	0.75 ± 0.19
$m(\tilde{\tau}, \tilde{\chi}_1^0) = (400, 1)$ GeV	4.59 ± 0.08	1.21 ± 0.04	3.38 ± 0.07	9.46 ± 0.12	2.08 ± 0.05	7.38 ± 0.10
p_0	0.5	-	-	0.5	-	-
Expected σ_{vis}^{95} [fb]	0.21	-	-	0.06	-	-
Observed σ_{vis}^{95} [fb]	0.17	-	-	0.04	-	-

SM process	SR-BDT3	SR-BDT3_bin0	SR-BDT3_bin1	SR-BDT4
Multi-boson	4.5 ± 2.1	2.0 ± 1.1	2.5 ± 1.3	1.8 ± 0.9
W+jets	$2.3^{+3.2}_{-2.3}$	$1.8^{+3.2}_{-1.8}$	0.5 ± 0.5	$0.01^{+0.68}_{-0.01}$
Top quark	3.7 ± 1.5	2.7 ± 1.3	1.0 ± 0.9	$0.16^{+0.19}_{-0.16}$
Z+jets	6.1 ± 3.5	$1.9^{+2.7}_{-1.9}$	4.1 ± 2.2	$0.25^{+0.92}_{-0.25}$
Higgs	0.12 ± 0.09	0.1 ± 0.1	$0.0^{+0.0}_{-0.0}$	0.01 ± 0.00
Multi-jet	0.02 ± 0.01	0.0 ± 0.0	0.0 ± 0.0	0.20 ± 0.07
SM total	17 ± 6	9 ± 5	8.2 ± 3.3	2.4 ± 1.4
Observed	7	6	1	1
$m(\tilde{\tau}, \tilde{\chi}_1^0) = (80, 1)$ GeV	10.8 ± 0.7	8.6 ± 0.7	2.19 ± 0.30	0.13 ± 0.07
$m(\tilde{\tau}, \tilde{\chi}_1^0) = (400, 1)$ GeV	9.39 ± 0.12	3.69 ± 0.07	5.70 ± 0.09	7.31 ± 0.10
p_0	0.5	-	-	0.5
Expected σ_{vis}^{95} [fb]	0.08	-	-	0.03
Observed σ_{vis}^{95} [fb]	0.05	-	-	0.03

The model-dependent fits using the results from the signal and control regions are used to place exclusion limits at 95% CL on direct stau production. SR-BDT4 has a low predicted yield, so 10,000 pseudoexperiments are used to calculate the exclusion limits. Since the four main SR-BDT overlap, the SR with the lowest expected CLs value for each signal scenario is used to set the limit, statistically combining the two bins each within SR-BDT1, SR-BDT2, and SR-BDT3 as two distinct regions. The exclusion limits for mass-degenerate $\tilde{\tau}_{L,R}$ production are shown in Figure 11(a), where stau masses up to 480 GeV are excluded for massless $\tilde{\chi}_1^0$. The limits are improved with respect to previous results, particularly towards

Table 10: Normalisation factors from the background-only fit in each scenario for the direct stau, intermediate stau, and intermediate Wh channels. The normalisation factors include corrections to the misidentified τ efficiency in addition to the cross-section and acceptance effects.

Channel	Direct stau	Intermediate stau			Intermediate Wh
Normalisation factor	$\tilde{\tau}\tilde{\tau}$	C1C1	C1N2OS	C1N2SS	C1N2Wh
$\mu_{W\text{+jets}}$	0.93 ± 0.11	0.98 ± 0.12	0.98 ± 0.12	1.04 ± 0.09	-
$\mu_{Z\text{+jets}}$	0.91 ± 0.07	-	-	-	-
μ_{Top}	0.85 ± 0.05	-	-	0.71 ± 0.11	1.00 ± 0.14
$\mu_{\text{Multi-jet}}$	-	1.0 ± 0.4	1.00 ± 0.29	1.00 ± 0.04	-

smaller $\tilde{\tau}$-$\tilde{\chi}_1^0$ mass splittings, as well as at higher $\tilde{\tau}$ masses. The observed limits are stronger than the expected limit due to the small observed deficit. The bump in the observed limit around stau masses of 350 GeV is due to a transition from one SR-BDT to another being used to set the limit.

The exclusion limits for $\tilde{\tau}_L$ and $\tilde{\tau}_R$ production separately are shown in Figure 11(b) and Figure 11(c), respectively. Similar improvements are seen in the sensitivity to $\tilde{\tau}_L$ production as for the mass-degenerate case, with stau masses excluded up to 410 GeV. Sensitivity to $\tilde{\tau}_R$ production is obtained for the first time at the LHC, with masses excluded up to 330 GeV.

10.2 Intermediate stau analysis

The observed number of events in each SR and the expected contributions from SM processes are given in Table 11. The contributions of multi-jet, W+jets and top quark events are scaled with the normalisation factors obtained from the background-only fit. The multi-jet normalisation with respect to the prediction from the ABCD method in all SRs is compatible with unity and has an uncertainty of 29–40 % (4 %), due to the small number of observed events in the multi-jet CR-A in C1C1 and C1N2OS (C1N2SS) scenarios. The W+jets normalisation factor is measured to be 0.98 ± 0.12 (1.04 ± 0.09) in C1C1 and C1N2OS (C1N2SS) scenarios and the top quark background normalisation factor is found to be 0.71 ± 0.11 in the C1N2SS scenario. The normalisation factors are summarised in Table 10. In all SRs, observations and background predictions are found to be compatible within uncertainties. The one-sided p_0-values, and the observed and expected 95 % CL upper limits on the visible non-SM cross-section (σ_{vis}^{95}) are shown. The accuracy of the limits obtained from the asymptotic formula was tested for all SRs by randomly generating a large number of pseudo-datasets and repeating the fit.

In the absence of a significant excess over the expected SM background, the observed and expected numbers of events in the signal regions are used to place exclusion limits at 95 % CL using the model-dependent fit. SR-C1C1-LM and SR-C1C1-HM are statistically combined to derive limits on $\tilde{\chi}_1^+\tilde{\chi}_1^-$ production, and SR-C1N2OS-LM, SR-C1N2OS-HM, SR-C1N2SS-LM and SR-C1N2SS-HM are combined to derive limits for the production of $\tilde{\chi}_1^+\tilde{\chi}_1^-$ and $\tilde{\chi}_1^\pm\tilde{\chi}_2^0$. The exclusion limits for simplified models are shown in Figure 12. Only $\tilde{\chi}_1^+\tilde{\chi}_1^-$ production is assumed for Figure 12 (a), whereas both production processes are considered simultaneously for the Figure 12 (b) and (c). The C1N2SS channel contributes significantly to the combination in the lower mass regions where this channel does not contain significant SM backgrounds.

Chargino masses up to 970 GeV are excluded for decays to a massless neutralino in the direct production of chargino pairs. For production of chargino pairs of mass-degenerate charginos and next-to-lightest

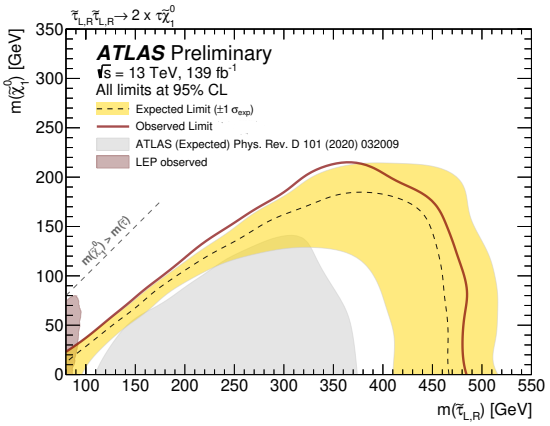

(a)

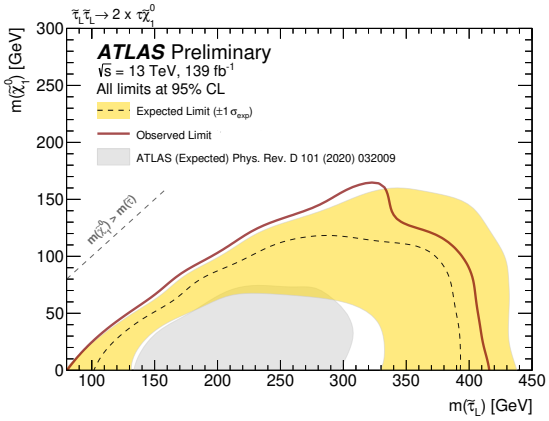

(b)

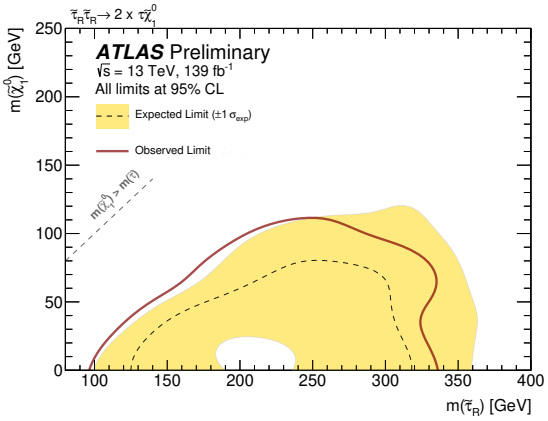

(c)

Figure 11: The 95% CL exclusion contours for simplified models of (a) $\tilde{\tau}_{L,R}\tilde{\tau}_{L,R}$ production, (b) $\tilde{\tau}_L\tilde{\tau}_L$ production, and (c) $\tilde{\tau}_R\tilde{\tau}_R$ production. The solid (dashed) lines show the observed (expected) exclusion contours. The band around the expected limit shows the $\pm 1\sigma$ variations, including all uncertainties except theoretical uncertainties in the signal cross-section. The expected exclusion contour from the previous ATLAS result in Ref. [15] is shown as a grey filled contour in (a) and (b).

neutralinos, chargino masses up to 1160 GeV are excluded for a massless neutralino. Both limits apply to scenarios where the neutralinos and charginos decay solely via intermediate staus and τ sneutrinos. These limits significantly extend previous results [14, 17] in the high $\tilde{\chi}_1^{\pm}/\tilde{\chi}_2^0$ mass region. The improvement at compressed and low $\tilde{\chi}_1^{\pm}/\tilde{\chi}_2^0$ masses is mainly driven by the C1N2SS analysis contribution.

10.3 Intermediate *Wh* analysis

The observed number of events in the two SRs and the expected contributions from SM processes are given in Table 12. The contribution of top quark background events is scaled with the normalisation factor obtained from the background-only fit. The top quark background normalisation factor is fitted to be 1.00 ± 0.14. In all SRs, the observed number of events from data and the background predictions are found to

Table 11: Observed and expected numbers of events for the background-only fit in the signal regions targeting chargino/neutralino production and decay via intermediate staus. Expected event yields for a few SUSY reference points are also shown. The uncertainties correspond to the sum in quadrature of statistical and systematic uncertainties. The correlation of systematic uncertainties among control regions and among background processes is taken into account. The one-sided p_0-values, and the observed and expected 95 % CL upper limits on the visible non-SM cross-section (σ_{vis}^{95}) from the model-independent fit are given.

SM process	SR-C1C1-LM	SR-C1C1-HM	SR-C1N2OS-LM	SR-C1N2OS-HM
Multi-boson	1.6 ± 0.6	2.2 ± 1.6	3.2 ± 1.2	2.4 ± 1.6
W+jets	0.4 ± 0.4	$0.29^{+0.35}_{-0.29}$	$0.6^{+2.2}_{-0.6}$	$0.29^{+0.35}_{-0.29}$
Top quark	1.0 ± 0.5	0.36 ± 0.13	$1.1^{+1.2}_{-1.1}$	0.36 ± 0.14
Z+jets	$1.4^{+1.5}_{-1.4}$	0.78 ± 0.34	2.5 ± 1.7	0.9 ± 0.4
Higgs	0.27 ± 0.06	$0.01^{+0.13}_{-0.01}$	0.40 ± 0.22	0.73 ± 0.23
Multi-jet	1.5 ± 0.5	0.37 ± 0.21	4.5 ± 1.0	0.31 ± 0.17
SM total	6.2 ± 2.0	4.0 ± 1.8	12.2 ± 4.8	5.0 ± 2.0
Observed	1	4	14	4
$m(\tilde{\chi}_1^{\pm}, \tilde{\chi}_1^0) = (700, 400)$ GeV	3.0 ± 0.6	7.8 ± 1.6	4.7 ± 1.0	14.1 ± 2.8
$m(\tilde{\chi}_1^{\pm}/\tilde{\chi}_2^0, \tilde{\chi}_1^0) = (1100, 0)$ GeV	0.20 ± 0.05	3.1 ± 0.6	0.39 ± 0.11	4.6 ± 1.0
p_0	0.5	0.5	0.4	0.5
Expected σ_{vis}^{95} [fb]	0.04	0.05	0.10	0.05
Observed σ_{vis}^{95} [fb]	0.02	0.05	0.10	0.05

SM process	SR-C1N2SS-LM	SR-C1N2SS-HM
Multi-boson	0.47 ± 0.20	0.8 ± 0.4
W+jets	0.33 ± 0.25	0.10 ± 0.05
Top quark	$0.01^{+0.02}_{-0.01}$	0.59 ± 0.20
Z+jets	0.20 ± 0.15	$0.6^{+0.8}_{-0.6}$
Higgs	$0.00^{+0.01}_{-0.00}$	0.02 ± 0.01
Multi-jet	0.9 ± 0.5	0.00 ± 0.00
SM total	2.0 ± 0.7	2.1 ± 1.1
Observed	2	3
$m(\tilde{\chi}_1^{\pm}/\tilde{\chi}_2^0, \tilde{\chi}_1^0) = (157, 92)$ GeV	4.6 ± 1.3	0.00 ± 0.00
p_0	0.4	0.3
Expected σ_{vis}^{95} [fb]	0.03	0.04
Observed σ_{vis}^{95} [fb]	0.03	0.04

be compatible within uncertainties. The one-sided p_0-values, the observed and expected 95 % CL upper limits on the visible non-SM cross-section (σ_{vis}^{95}) are shown.

Since no significant excess over the expected SM background is observed, the observed and expected number of events in the SRs are used to place exclusion limits at 95 % CL using the model-dependent fit. The best expected limits for SR-Wh-LM and SR-Wh-HM are used to derive limits on $\tilde{\chi}_1^{\pm}\tilde{\chi}_2^0$ production decaying via an intermediate Wh, and are shown in Figure 13. Gaugino masses up to 330 GeV are excluded for a massless lightest neutralino.

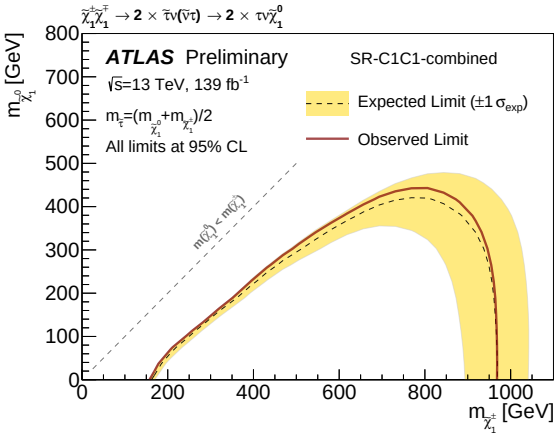

(a)

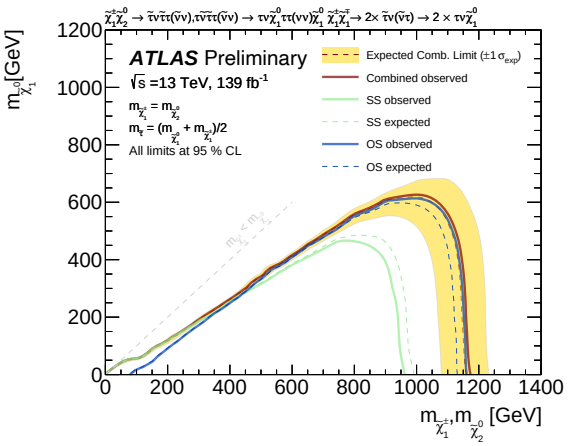

(b)

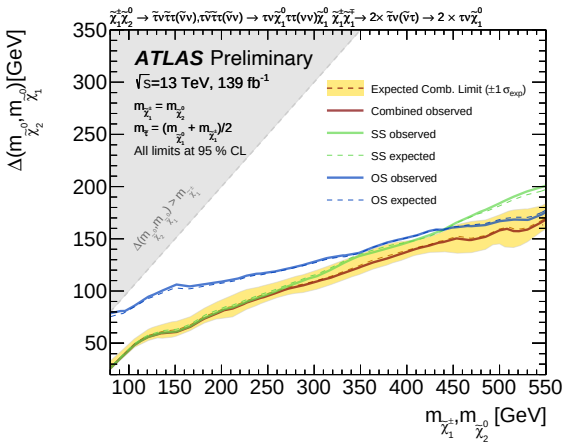

(c)

Figure 12: The 95 % CL exclusion contours for simplified models of (a) $\tilde{\chi}_1^+\tilde{\chi}_1^-$ production, and of (b-c) $\tilde{\chi}_1^+\tilde{\chi}_1^-$ and $\tilde{\chi}_1^\pm\tilde{\chi}_2^0$ production. The solid (dashed) lines show the observed (expected) exclusion contours. The band around the expected limit shows the $\pm 1\sigma$ variations, including all uncertainties except theoretical uncertainties in the signal cross-section. The green curves are from the contribution of C1N2SS scenario, while the blue curves are from the contribution of C1C1 and C1N2OS scenarios, and the red curves are the combination of the channels. The grey solid area in (c) shows the forbidden area where $m(\tilde{\chi}_1^0) > m(\tilde{\chi}_2^0)$.

Table 12: Observed and expected numbers of events for the background-only fit in the signal regions targeting chargino-neutralino production and decay via Wh. Expected event yields for a few SUSY reference points are also shown. The uncertainties correspond to the sum in quadrature of statistical and systematic uncertainties. The correlation of systematic uncertainties among control regions and among background processes is fully taken into account. The one-sided p_0-values, and the observed and expected 95 % CL upper limits on the visible non-SM cross-section (σ_{vis}^{95}) from the model-independent fit are given.

SM process	SR-Wh-LM	SR-Wh-HM
Multi-boson	1.85 ± 0.5	1.1 ± 0.4
Misidentified processes	1.4 ± 0.6	0.06 ± 0.03
Top quark	1.9 ± 0.6	$0.04^{+0.06}_{-0.04}$
Z+jets	0.05 ± 0.02	0.03 ± 0.01
Higgs	$0.13^{+0.99}_{-0.13}$	0.06 ± 0.02
SM total	5.3 ± 1.4	1.3 ± 0.4
Observed	4	2
$m(\tilde{\chi}_1^{\pm}/\tilde{\chi}_2^0, \tilde{\chi}_1^0) = (225, 75)$ GeV	5.8 ± 1.5	3.3 ± 0.9
p_0	0.5	0.3
Expected σ_{vis}^{95} [fb]	0.05	0.03
Observed σ_{vis}^{95} [fb]	0.04	0.03

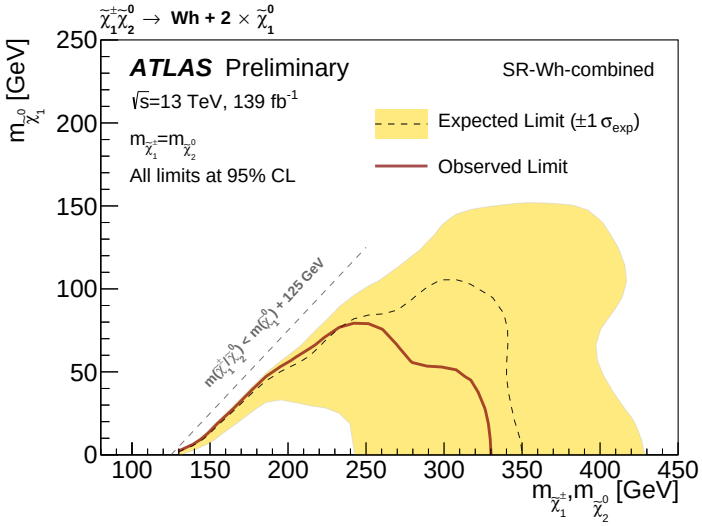

Figure 13: The 95 % CL exclusion contours for simplified models of $\tilde{\chi}_1^{\pm}\tilde{\chi}_2^0$ production decaying via an intermediate Wh. The solid (dashed) lines show the observed (expected) exclusion contours. The band around the expected limit shows the $\pm 1\sigma$ variations, including all uncertainties except theoretical uncertainties in the signal cross-section. The best expected limits for SR-Wh-LM and SR-Wh-HM are used.

11 Conclusion

Searches for direct stau production, direct gaugino pair production decaying via an intermediate stau or Wh with at least two hadronically decaying taus in the final state have been presented. The searches use 139 fb^{-1} of integrated luminosity of pp collisions at $\sqrt{s}$ = 13 TeV collected by the ATLAS detector from 2015 to 2018. Agreement between data and SM expectation is observed in all signal regions and the results are used to set limits on the visible cross-section for events beyond the Standard Model. Exclusion limits at 95% CL are also placed on simplified models of direct stau production, excluding mass-degenerate $\tilde{\tau}_{L,R}$ up to 480 GeV, $\tilde{\tau}_L$ up to 410 GeV, and $\tilde{\tau}_R$ up to 330 GeV. The sensitivity to $\tilde{\tau}_R\tilde{\tau}_R$ production obtained here is the first from the LHC, achieved through the use of a BDT for improved signal-background separation.

In the scenario of direct production of wino-like chargino pairs decaying into the lightest neutralino via an intermediate on-shell stau, exclusion limits are placed for chargino masses up to 970 GeV for a massless lightest neutralino. In the case of associated production of pairs of charginos and pairs of degenerate charginos and next-to-lightest neutralinos, masses up to 1160 GeV are excluded for a massless lightest neutralino. These limits improve upon previous results by 340-400 GeV, mainly due to an increased amount of integrated luminosity and improvements in the recurrent neural network τ identification. The sensitivity for more compressed mass scenarios is also improved by the addition of the same-sign τ channel and the use of BDTs for stau production. For pairs of degenerate charginos and next-to-lightest neutralinos via Wh decay production, gaugino masses up to 330 GeV are excluded for a massless lightest neutralino. Gaugino masses up to 330 GeV are excluded for production of a lightest chargino and a next-to-lightest neutralino, both decaying via Wh, assuming the $\tilde{\chi}_1^{\pm}$ and $\tilde{\chi}_2^0$ have equal masses and the lightest neutralino is massless.

Acknowledgements

We thank CERN for the very successful operation of the LHC, as well as the support staff from our institutions without whom ATLAS could not be operated efficiently.

We acknowledge the support of ANPCyT, Argentina; YerPhI, Armenia; ARC, Australia; BMWFW and FWF, Austria; ANAS, Azerbaijan; CNPq and FAPESP, Brazil; NSERC, NRC and CFI, Canada; CERN; ANID, Chile; CAS, MOST and NSFC, China; Minciencias, Colombia; MEYS CR, Czech Republic; DNRF and DNSRC, Denmark; IN2P3-CNRS and CEA-DRF/IRFU, France; SRNSFG, Georgia; BMBF, HGF and MPG, Germany; GSRI, Greece; RGC and Hong Kong SAR, China; ISF and Benoziyo Center, Israel; INFN, Italy; MEXT and JSPS, Japan; CNRST, Morocco; NWO, Netherlands; RCN, Norway; MEiN, Poland; FCT, Portugal; MNE/IFA, Romania; MESTD, Serbia; MSSR, Slovakia; ARRS and MIZŠ, Slovenia; DSI/NRF, South Africa; MICINN, Spain; SRC and Wallenberg Foundation, Sweden; SERI, SNSF and Cantons of Bern and Geneva, Switzerland; MOST, Taiwan; TENMAK, Türkiye; STFC, United Kingdom; DOE and NSF, United States of America. In addition, individual groups and members have received support from BCKDF, CANARIE, Compute Canada and CRC, Canada; PRIMUS 21/SCI/017 and UNCE SCI/013, Czech Republic; COST, ERC, ERDF, Horizon 2020 and Marie Skłodowska-Curie Actions, European Union; Investissements d'Avenir Labex, Investissements d'Avenir Idex and ANR, France; DFG and AvH Foundation, Germany; Herakleitos, Thales and Aristeia programmes co-financed by EU-ESF and the Greek NSRF, Greece; BSF-NSF and MINERVA, Israel; Norwegian Financial Mechanism 2014-2021, Norway; NCN and NAWA, Poland; La Caixa Banking Foundation, CERCA Programme Generalitat de Catalunya and PROMETEO and GenT Programmes Generalitat Valenciana, Spain; Göran Gustafssons Stiftelse, Sweden; The Royal Society and Leverhulme Trust, United Kingdom.

The crucial computing support from all WLCG partners is acknowledged gratefully, in particular from CERN, the ATLAS Tier-1 facilities at TRIUMF (Canada), NDGF (Denmark, Norway, Sweden), CC-IN2P3 (France), KIT/GridKA (Germany), INFN-CNAF (Italy), NL-T1 (Netherlands), PIC (Spain), ASGC (Taiwan), RAL (UK) and BNL (USA), the Tier-2 facilities worldwide and large non-WLCG resource providers. Major contributors of computing resources are listed in Ref. [93].

References

[1] Y. Golfand and E. Likhtman,
Extension of the Algebra of Poincare Group Generators and Violation of P Invariance,
JETP Lett. **13** (1971) 323, [Pisma Zh. Eksp. Teor. Fiz. **13** (1971) 452].

[2] D. Volkov and V. Akulov, *Is the neutrino a goldstone particle?*, Phys. Lett. B **46** (1973) 109.

[3] J. Wess and B. Zumino, *Supergauge transformations in four dimensions*,
Nucl. Phys. B **70** (1974) 39.

[4] J. Wess and B. Zumino, *Supergauge invariant extension of quantum electrodynamics*,
Nucl. Phys. B **78** (1974) 1.

[5] S. Ferrara and B. Zumino, *Supergauge invariant Yang-Mills theories*, Nucl. Phys. B **79** (1974) 413.

[6] A. Salam and J. Strathdee, *Super-symmetry and non-Abelian gauges*, Phys. Lett. B **51** (1974) 353.

[7] S. P. Martin, *A Supersymmetry Primer*, Adv. Ser. Direct. High Energy Phys. **18** (1998) 1,
arXiv: hep-ph/9709356.

[8] G. R. Farrar and P. Fayet, *Phenomenology of the production, decay, and detection of new hadronic states associated with supersymmetry*, Phys. Lett. B **76** (1978) 575.

[9] H. Goldberg, *Constraint on the Photino Mass from Cosmology*, Phys. Rev. Lett. **50** (1983) 1419,
Erratum: Phys. Rev. Lett. **103** (2009) 099905.

[10] J. Ellis, J. Hagelin, D. V. Nanopoulos, K. A. Olive and M. Srednicki,
Supersymmetric relics from the big bang, Nucl. Phys. B **238** (1984) 453.

[11] D. Albornoz Vásquez, G. Bélanger and C. Bœhm,
Revisiting light neutralino scenarios in the MSSM, Phys. Rev. D **84** (2011) 095015,
arXiv: 1108.1338 [hep-ph].

[12] ATLAS Collaboration, *Search for the direct production of charginos, neutralinos and staus in final states with at least two hadronically decaying taus and missing transverse momentum in pp collisions at $\sqrt{s} = 8$ TeV with the ATLAS detector*, JHEP **10** (2014) 096,
arXiv: 1407.0350 [hep-ex].

[13] ATLAS Collaboration, *Search for the electroweak production of supersymmetric particles in $\sqrt{s} = 8$ TeV pp collisions with the ATLAS detector*, Phys. Rev. D **93** (2016) 052002,
arXiv: 1509.07152 [hep-ex].

[14] ATLAS Collaboration, *Search for the direct production of charginos and neutralinos in final states with tau leptons in $\sqrt{s} = 13$ TeV pp collisions with the ATLAS detector*,
Eur. Phys. J. C **78** (2018) 154, arXiv: 1708.07875 [hep-ex].

[15] ATLAS Collaboration, *Search for direct stau production in events with two hadronic τ-leptons in $\sqrt{s} = 13$ TeV pp collisions with the ATLAS detector*, Phys. Rev. D **101** (2020) 032009,
arXiv: 1911.06660 [hep-ex].

[16] CMS Collaboration, *Search for direct pair production of supersymmetric partners of τ leptons in the final state with two hadronically decaying τ leptons and missing transverse momentum in proton–proton collisions at $\sqrt{s}$ = 13 TeV*, (2022), arXiv: 2207.02254 [hep-ex].

[17] CMS Collaboration, *Search for electroweak production of charginos and neutralinos in proton–proton collisions at $\sqrt{s}$ = 13 TeV*, JHEP **04** (2021) 147, arXiv: 2106.14246 [hep-ex].

[18] ATLAS Collaboration, *The ATLAS Experiment at the CERN Large Hadron Collider*, JINST **3** (2008) S08003.

[19] ATLAS Collaboration, *The ATLAS Collaboration Software and Firmware*, ATL-SOFT-PUB-2021-001, 2021, URL: https://cds.cern.ch/record/2767187.

[20] ATLAS Collaboration, *ATLAS data quality operations and performance for 2015–2018 data-taking*, JINST **15** (2020) P04003, arXiv: 1911.04632 [physics.ins-det].

[21] T. Sjöstrand, S. Mrenna and P. Z. Skands, *A brief introduction to PYTHIA 8.1*, Comput. Phys. Commun. **178** (2008) 852, arXiv: 0710.3820 [hep-ph].

[22] ATLAS Collaboration, *The Pythia 8 A3 tune description of ATLAS minimum bias and inelastic measurements incorporating the Donnachie–Landshoff diffractive model*, ATL-PHYS-PUB-2016-017, 2016, URL: https://cds.cern.ch/record/2206965.

[23] R. D. Ball et al., *Parton distributions with LHC data*, Nucl. Phys. B **867** (2013) 244, arXiv: 1207.1303 [hep-ph].

[24] D. J. Lange, *The EvtGen particle decay simulation package*, Nucl. Instrum. Meth. A **462** (2001) 152.

[25] ATLAS Collaboration, *The ATLAS Simulation Infrastructure*, Eur. Phys. J. C **70** (2010) 823, arXiv: 1005.4568 [physics.ins-det].

[26] GEANT4 Collaboration, S. Agostinelli et al., *GEANT4 – a simulation toolkit*, Nucl. Instrum. Meth. A **506** (2003) 250.

[27] ATLAS Collaboration, *Performance of the Fast ATLAS Tracking Simulation (FATRAS) and the ATLAS Fast Calorimeter Simulation (FastCaloSim) with single particles*, ATL-SOFT-PUB-2014-001, 2014, URL: https://cds.cern.ch/record/1669341.

[28] S. Frixione, P. Nason and G. Ridolfi, *A positive-weight next-to-leading-order Monte Carlo for heavy flavour hadroproduction*, JHEP **09** (2007) 126, arXiv: 0707.3088 [hep-ph].

[29] P. Nason, *A new method for combining NLO QCD with shower Monte Carlo algorithms*, JHEP **11** (2004) 040, arXiv: hep-ph/0409146.

[30] S. Frixione, P. Nason and C. Oleari, *Matching NLO QCD computations with Parton Shower simulations: the POWHEG method*, JHEP **11** (2007) 070, arXiv: 0709.2092 [hep-ph].

[31] S. Alioli, P. Nason, C. Oleari and E. Re, *A general framework for implementing NLO calculations in shower Monte Carlo programs: the POWHEG BOX*, JHEP **06** (2010) 043, arXiv: 1002.2581 [hep-ph].

[32] ATLAS Collaboration, *ATLAS Pythia 8 tunes to 7 TeV data*, ATL-PHYS-PUB-2014-021, 2014, URL: https://cds.cern.ch/record/1966419.

[33] M. Beneke, P. Falgari, S. Klein and C. Schwinn,
Hadronic top-quark pair production with NNLL threshold resummation,
Nucl. Phys. B **855** (2012) 695, arXiv: 1109.1536 [hep-ph].

[34] M. Cacciari, M. Czakon, M. Mangano, A. Mitov and P. Nason, *Top-pair production at hadron colliders with next-to-next-to-leading logarithmic soft-gluon resummation*,
Phys. Lett. B **710** (2012) 612, arXiv: 1111.5869 [hep-ph].

[35] P. Bärnreuther, M. Czakon and A. Mitov, *Percent-Level-Precision Physics at the Tevatron: Next-to-Next-to-Leading Order QCD Corrections to $q\bar{q} \to t\bar{t} + X$*,
Phys. Rev. Lett. **109** (2012) 132001, arXiv: 1204.5201 [hep-ph].

[36] M. Czakon and A. Mitov,
NNLO corrections to top-pair production at hadron colliders: the all-fermionic scattering channels,
JHEP **12** (2012) 054, arXiv: 1207.0236 [hep-ph].

[37] M. Czakon and A. Mitov,
NNLO corrections to top pair production at hadron colliders: the quark-gluon reaction,
JHEP **01** (2013) 080, arXiv: 1210.6832 [hep-ph].

[38] M. Czakon, P. Fiedler and A. Mitov,
Total Top-Quark Pair-Production Cross Section at Hadron Colliders Through $O(\alpha_S^4)$,
Phys. Rev. Lett. **110** (2013) 252004, arXiv: 1303.6254 [hep-ph].

[39] M. Czakon and A. Mitov,
Top++: A program for the calculation of the top-pair cross-section at hadron colliders,
Comput. Phys. Commun. **185** (2014) 2930, arXiv: 1112.5675 [hep-ph].

[40] M. Aliev et al., *HATHOR – HAdronic Top and Heavy quarks crOss section calculatoR*,
Comput. Phys. Commun. **182** (2011) 1034, arXiv: 1007.1327 [hep-ph].

[41] P. Kant et al., *HatHor for single top-quark production: Updated predictions and uncertainty estimates for single top-quark production in hadronic collisions*,
Comput. Phys. Commun. **191** (2015) 74, arXiv: 1406.4403 [hep-ph].

[42] J. Alwall et al., *The automated computation of tree-level and next-to-leading order differential cross sections, and their matching to parton shower simulations*, JHEP **07** (2014) 079,
arXiv: 1405.0301 [hep-ph].

[43] A. Lazopoulos, T. McElmurry, K. Melnikov and F. Petriello,
Next-to-leading order QCD corrections to $t\bar{t}Z$ production at the LHC, Phys. Lett. B **666** (2008) 62,
arXiv: 0804.2220 [hep-ph].

[44] J. M. Campbell and R. K. Ellis, *$t\bar{t}W^{+-}$ production and decay at NLO*, JHEP **07** (2012) 052,
arXiv: 1204.5678 [hep-ph].

[45] T. Gleisberg et al., *Event generation with SHERPA 1.1*, JHEP **02** (2009) 007,
arXiv: 0811.4622 [hep-ph].

[46] S. Höche, F. Krauss, M. Schonherr and F. Siegert,
QCD matrix elements + parton showers: The NLO case, JHEP **04** (2013) 027,
arXiv: 1207.5030 [hep-ph].

[47] T. Gleisberg and S. Höche, *Comix, a new matrix element generator*, JHEP **12** (2008) 039,
arXiv: 0808.3674 [hep-ph].

[48] F. Cascioli, P. Maierhofer and S. Pozzorini, *Scattering Amplitudes with Open Loops*, Phys. Rev. Lett. **108** (2012) 111601, arXiv: 1111.5206 [hep-ph].

[49] A. Denner, S. Dittmaier and L. Hofer, *Collier: a fortran-based Complex One-Loop LIbrary in Extended Regularizations*, Comput. Phys. Commun. **212** (2017) 220, arXiv: 1604.06792 [hep-ph].

[50] S. Schumann and F. Krauss, *A Parton shower algorithm based on Catani-Seymour dipole factorisation*, JHEP **03** (2008) 038, arXiv: 0709.1027 [hep-ph].

[51] R. D. Ball et al., *Parton distributions for the LHC Run II*, JHEP **04** (2015) 040, arXiv: 1410.8849 [hep-ph].

[52] S. Catani, L. Cieri, G. Ferrera, D. de Florian and M. Grazzini, *Vector Boson Production at Hadron Colliders: A Fully Exclusive QCD Calculation at Next-to-Next-to-Leading Order*, Phys. Rev. Lett. **103** (2009) 082001, arXiv: 0903.2120 [hep-ph].

[53] S. Höche, F. Krauss, M. Schonherr and F. Siegert, *A critical appraisal of NLO+PS matching methods*, JHEP **09** (2012) 049, arXiv: 1111.1220 [hep-ph].

[54] S. Catani, F. Krauss, R. Kuhn and B. R. Webber, *QCD matrix elements + parton showers*, JHEP **11** (2001) 063, arXiv: hep-ph/0109231.

[55] S. Höche, F. Krauss, S. Schumann and F. Siegert, *QCD matrix elements and truncated showers*, JHEP **05** (2009) 053, arXiv: 0903.1219 [hep-ph].

[56] D. de Florian et al., *Handbook of LHC Higgs Cross Sections: 4. Deciphering the Nature of the Higgs Sector*, 2016, arXiv: 1610.07922 [hep-ph].

[57] L. Lönnblad and S. Prestel, *Matching tree-level matrix elements with interleaved showers*, JHEP **03** (2012) 019, arXiv: 1109.4829 [hep-ph].

[58] B. Fuks, M. Klasen, D. R. Lamprea and M. Rothering, *Gaugino production in proton-proton collisions at a center-of-mass energy of* 8 *TeV*, JHEP **10** (2012) 081, arXiv: 1207.2159 [hep-ph].

[59] B. Fuks, M. Klasen, D. R. Lamprea and M. Rothering, *Precision predictions for electroweak superpartner production at hadron colliders with* RESUMMINO, Eur. Phys. J. C **73** (2013) 2480, arXiv: 1304.0790 [hep-ph].

[60] C. Borschensky et al., *Squark and gluino production cross sections in pp collisions at* $\sqrt{s} = 13, 14, 33$ *and* 100 *TeV*, Eur. Phys. J. C **74** (2014) 3174, arXiv: 1407.5066 [hep-ph].

[61] ATLAS Collaboration, *Vertex Reconstruction Performance of the ATLAS Detector at* $\sqrt{s} = 13$ *TeV*, ATL-PHYS-PUB-2015-026, 2015, URL: https://cds.cern.ch/record/2037717.

[62] ATLAS Collaboration, *Jet reconstruction and performance using particle flow with the ATLAS Detector*, Eur. Phys. J. C **77** (2017) 466, arXiv: 1703.10485 [hep-ex].

[63] M. Cacciari, G. P. Salam and G. Soyez, *The anti-k_t jet clustering algorithm*, JHEP **04** (2008) 063, arXiv: 0802.1189 [hep-ph].

[64] M. Cacciari, G. P. Salam and G. Soyez, *FastJet user manual*, Eur. Phys. J. C **72** (2012) 1896, arXiv: 1111.6097 [hep-ph].

[65] ATLAS Collaboration, *Jet energy measurement with the ATLAS detector in proton–proton collisions at* $\sqrt{s} = 7$ *TeV*, Eur. Phys. J. C **73** (2013) 2304, arXiv: 1112.6426 [hep-ex].

[66] ATLAS Collaboration, *Jet Calibration and Systematic Uncertainties for Jets Reconstructed in the ATLAS Detector at* $\sqrt{s} = 13$ *TeV*, ATL-PHYS-PUB-2015-015, 2015, URL: https://cds.cern.ch/record/2037613.

[67] M. Cacciari and G. P. Salam, *Pileup subtraction using jet areas*, Phys. Lett. B **659** (2008) 119, arXiv: 0707.1378.

[68] ATLAS Collaboration, *Performance of pile-up mitigation techniques for jets in* pp *collisions at* $\sqrt{s} = 8$ *TeV using the ATLAS detector*, Eur. Phys. J. C **76** (2016) 581, arXiv: 1510.03823 [hep-ex].

[69] ATLAS Collaboration, *Selection of jets produced in* 13 *TeV proton–proton collisions with the ATLAS detector*, ATLAS-CONF-2015-029, 2015, URL: https://cds.cern.ch/record/2037702.

[70] ATLAS Collaboration, *Optimisation and performance studies of the ATLAS b-tagging algorithms for the 2017-18 LHC run*, ATL-PHYS-PUB-2017-013, 2017, URL: https://cds.cern.ch/record/2273281.

[71] ATLAS Collaboration, *ATLAS b-jet identification performance and efficiency measurement with* $t\bar{t}$ *events in* pp *collisions at* $\sqrt{s} = 13$ *TeV*, Eur. Phys. J. C **79** (2019) 970, arXiv: 1907.05120 [hep-ex].

[72] ATLAS Collaboration, *Electron and photon performance measurements with the ATLAS detector using the 2015–2017 LHC proton–proton collision data*, JINST **14** (2019) P12006, arXiv: 1908.00005 [hep-ex].

[73] ATLAS Collaboration, *Muon reconstruction and identification efficiency in ATLAS using the full Run 2* pp *collision data set at* $\sqrt{s} = 13$ *TeV*, Eur. Phys. J. C **81** (2021) 578, arXiv: 2012.00578 [hep-ex].

[74] ATLAS Collaboration, *Measurement of the tau lepton reconstruction and identification performance in the ATLAS experiment using* pp *collisions at* $\sqrt{s} = 13$ *TeV*, ATLAS-CONF-2017-029, 2017, URL: https://cds.cern.ch/record/2261772.

[75] ATLAS Collaboration, *Reconstruction, Energy Calibration, and Identification of Hadronically Decaying Tau Leptons in the ATLAS Experiment for Run-2 of the LHC*, ATL-PHYS-PUB-2015-045, 2015, URL: https://cds.cern.ch/record/2064383.

[76] ATLAS Collaboration, *Identification of hadronic tau lepton decays using neural networks in the ATLAS experiment*, ATL-PHYS-PUB-2019-033, 2019, URL: https://cds.cern.ch/record/2688062.

[77] ATLAS Collaboration, *Identification and energy calibration of hadronically decaying tau leptons with the ATLAS experiment in* pp *collisions at* $\sqrt{s} = 8$ *TeV*, Eur. Phys. J. C **75** (2015) 303, arXiv: 1412.7086 [hep-ex].

[78] ATLAS Collaboration, *Expected performance of missing transverse momentum reconstruction for the ATLAS detector at* $\sqrt{s} = 13$ *TeV*, ATL-PHYS-PUB-2015-023, 2015, URL: https://cds.cern.ch/record/2037700.

[79] ATLAS Collaboration, *Performance of missing transverse momentum reconstruction with the ATLAS detector in the first proton–proton collisions at* $\sqrt{s}$ = 13 *TeV*, ATL-PHYS-PUB-2015-027, 2015, URL: https://cds.cern.ch/record/2037904.

[80] C. G. Lester and D. J. Summers, *Measuring masses of semi-invisibly decaying particles pair produced at hadron colliders*, Phys. Lett. B **463** (1999) 99, arXiv: hep-ph/9906349.

[81] A. Barr, C. Lester and P. Stephens, *A variable for measuring masses at hadron colliders when missing energy is expected; m_{T2}: the truth behind the glamour*, J. Phys. G **29** (2003) 2343, arXiv: hep-ph/0304226.

[82] G. Ke et al., *LightGBM: A Highly Efficient Gradient Boosting Decision Tree*, NIPS'17 (2017) 3149.

[83] ATLAS Collaboration, *Performance of the ATLAS muon triggers in Run 2*, JINST **15** (2020) P09015, arXiv: 2004.13447 [hep-ex].

[84] D. Tovey, *On measuring the masses of pair-produced semi-invisibly decaying particles at hadron colliders*, JHEP **04** (2008) 034, arXiv: 0802.2879.

[85] ATLAS Collaboration, *E_T^{miss} performance in the ATLAS detector using 2015–2016 LHC pp collisions*, ATLAS-CONF-2018-023, 2018, URL: https://cds.cern.ch/record/2625233.

[86] ATLAS Collaboration, *Measurement of the Inelastic Proton-Proton Cross Section at* $\sqrt{s} = 13$ *TeV with the ATLAS Detector at the LHC*, Phys. Rev. Lett. **117** (2016) 182002, arXiv: 1606.02625 [hep-ex].

[87] ATLAS Collaboration, *Luminosity determination in pp collisions at* $\sqrt{s}$ = 13 *TeV using the ATLAS detector at the LHC*, ATLAS-CONF-2019-021, 2019, URL: https://cds.cern.ch/record/2677054.

[88] G. Avoni et al., *The new LUCID-2 detector for luminosity measurement and monitoring in ATLAS*, JINST **13** (2018) 07017.

[89] J. Butterworth et al., *PDF4LHC recommendations for LHC Run II*, J. Phys. G **43** (2016) 023001, arXiv: 1510.03865 [hep-ex].

[90] M. Baak et al., *HistFitter software framework for statistical data analysis*, Eur. Phys. J. C **75** (2015) 153, arXiv: 1410.1280 [hep-ex].

[91] G. Cowan, K. Cranmer, E. Gross and O. Vitells, *Asymptotic formulae for likelihood-based tests of new physics*, Eur. Phys. J. C **71** (2011) 1554, [Erratum: Eur. Phys. J. C **73** (2013) 2501], arXiv: 1007.1727 [physics.data-an], [Erratum: Eur. Phys. J. C **73** (2013) 2501].

[92] A. L. Read, *Presentation of search results: the CL_s technique*, J. Phys. G **28** (2002) 2693.

[93] ATLAS Collaboration, *ATLAS Computing Acknowledgements*, ATL-SOFT-PUB-2021-003, 2021, URL: https://cds.cern.ch/record/2776662.

Auxiliary material

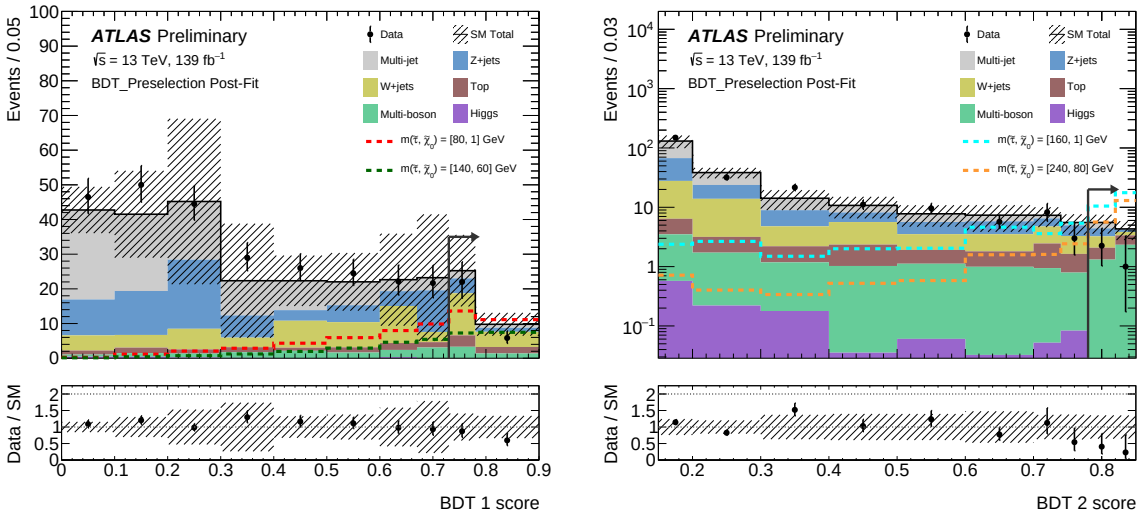

(a) (b)

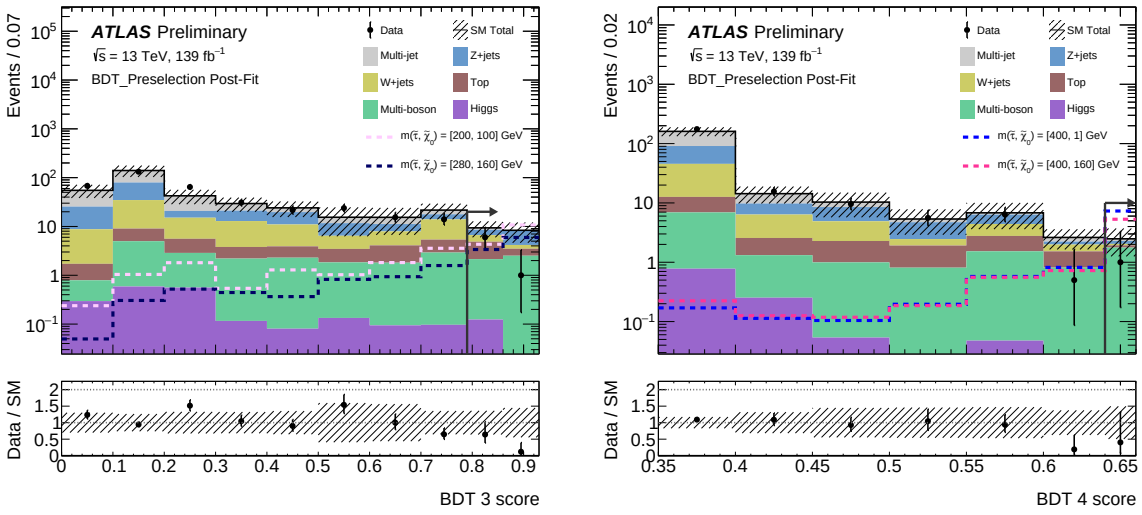

(c) (d)

Figure 14: The post-fit BDT score distributions for the direct stau channel, showing the scores for (a) BDT1, (b) BDT2, (c) BDT3, and (d) BDT4, before the selections on the BDT scores are made. The black arrow depicts the BDT score selection for the SR-BDT. A few example SUSY scenarios targeted by each BDT are overlaid for illustration. The hashed bands represent the combined statistical and systematic uncertainties of the total SM background. The lower panels show the ratio of data to the total SM background estimate.